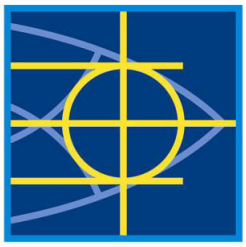

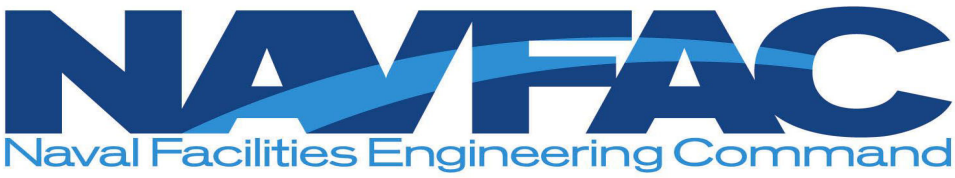


**ENGINEERING SERVICE CENTER**
**Port Hueneme, California 93043-4370**

# TECHNICAL MEMORANDUM
## TM-2378-AMP

# STABILITY ASSESSMENT OF MHP TEST BED FOR OCEAN TOW

By

Erick T. Huang

January 2005

# REPORT DOCUMENTATION PAGE

*Form Approved*
*OMB No. 0704-0811*



| 1. REPORT DATE *(DD-MM-YYYY)* | 2. REPORT TYPE | 3. DATES COVERED *(From – To)* |
|---|---|---|
| January 2005 | Final | N/A |

**4. TITLE AND SUBTITLE**

**STABILITY ASSESSMENT OF MHP TEST BED FOR OCEAN TOW**

**5a. CONTRACT NUMBER**

**5b. GRANT NUMBER**

**5c. PROGRAM ELEMENT NUMBER**

**6. AUTHOR(S)**

Erick T. Huang

**5d. PROJECT NUMBER**

**5e. TASK NUMBER**

**5f. WORK UNIT NUMBER**

**7. PERFORMING ORGANIZATION NAME(S) AND ADDRESSES**

Commander
Naval Facilities Engineering Service Center
1100 23rd Avenue
Port Hueneme, CA 93043

**8. PERFORMING ORGANIZATION REPORT NUMBER**

TM-2378-AMP

**9. SPONSORING/MONITORING AGENCY NAME(S) AND ADDRESS(ES)**

**10. SPONSOR/MONITORS ACRONYM(S)**

**11. SPONSOR/MONITOR'S REPORT NUMBER(S)**

**12. DISTRIBUTION/AVAILABILITY STATEMENT**

**13. SUPPLEMENTARY NOTES**

**14. ABSTRACT**

This task reviews the ultimate stability of a heavy concrete platform under tow along the west coast of the United States. Two hull configurations of the platform are assessed for their seaway thresholds based on their static stability curves and dynamic performances. The dynamic performances are determined with a time domain simulation model built on a large amplitude motion scheme that closely tracks the instant wetted hull shape and fluid forces including viscous damping. Heavy seas heave the platform wildly and occasionally engulf the entire platform of both configurations. Simulation results indicate that the platform as designed may capsize in low sea state 5. The capsizing is largely attributed to a total loss of static stability due to severe deck immersion that allows the platform to heel extensively and eventually capsizes. The same platform with a quadruple freeboard extends its operation window substantially to Sea State 7. The stability assessment procedure and its rational basis are documented.

**15. SUBJECT TERMS**

Modular Hybrid Pier (MHP), ship, freeboard, stability assessment

| 16. SECURITY CLASSIFICATION OF: | | | 17. LIMITATION OF ABSTRACT | 18. NUMBER OF PAGES | 19a. NAME OF RESPONSIBLE PERSON |
|---|---|---|---|---|---|
| a. REPORT | b. ABSTRACT | c. THIS PAGE | | | 19b. TELEPHONE NUMBER *(include area code)* |
| U | U | U | U | 65 | |

**Standard Form 298** (Rev. 8/98)
Prescribed by ANSI Std. Z39.18

## EXECUTIVE SUMMARY

The stability of a ship is the ability to stay upright in the most robust and efficient attitude as designed. In general, hull form and mass inertia property determine the stability capacity of a ship, and the nature of the seaway decides if this capacity is sufficient. A ship with a wider hull and a lower center of gravity is more stable, allowing it to survive a higher seaway.

The objective of this task was to review the ultimate stability of a short Test Bed of the Modular Hybrid Pier (MHP) in open seaways. It is desirable that the test bed remains upright, because its structural integrity and water tightness in an upside down attitude are uncertain. Although seaways en route are relatively clam in the summer season, offshore weather stations report waves above 10 feet from time-to-time and exceeding 20 feet occasionally. Since safe havens are out of reach on the journey, safety of the operation heavily depends on the inherent stability of the Test Bed. However, this platform is only conditionally stable due to a high center of gravity. Although the wide, flat hull of this platform presents a high initial stability, it also renders the platform highly wave sensitive. Its stability capacity varies dramatically as the wetted hull shape constantly changes in heavy seas. Capsizing is a legitimate concern.

Existing stability criteria are established on a static basis and are often hull specific. These criteria provide general guidelines for preparing reasonable stability for a ship but fall short for resolving the ultimate stability of a ship under specific conditions. This study attempted to identify the seaway thresholds of the Test Bed by directly inspecting its dynamic performance in the target seaways with a time domain simulation code. This code closely tracks the instant wet hull geometry and fluid forces, including viscous damping, and, therefore, is capable of tracing the platform responses up to capsizing. A parametric study was conducted to confirm the performance of this code and subsequently design a realistic numerical model that best represents the ocean tow scenario. This code was then used to explore the capsizing process and Test Bed performance in heavy seas. The results were further compiled to determine the threshold seaways that the Test Bed can possibly withstand during ocean tow.

Two hull configurations were assessed for the ocean tow. One retained the configuration as designed and the other closed the entire space between the service and operation decks watertight. Simulation results indicated that the Test Bed as designed may capsize in low Sea State 5. The capsizing is largely attributed to a total loss of static stability due to severe immersion of the service deck, which allowed the Test Bed to heel beyond the range of positive righting arms. The revised configuration, with a quadruple freeboard, greatly enhanced the ultimate stability above Sea State 6. Nevertheless, high sea states heaved the revised hull extensively and often engulfed the entire platform momentarily. Fortunately, the revised hull in full immersion presents a slight, positive stability and, therefore, is unlikely to capsize. The revised Test Bed, with proper routing selection, should have a good chance of survival during the intended ocean tow, provided that all pontoons remain watertight.

TABLE OF CONTENTS

## INTRODUCTION

### Objective

The objective of this study was to determine the ultimate stability of the Modular Hybrid Pier (MHP) Test Bed in heavy seaways. The results will be used to prepare the Test Bed for ocean tow from Seattle, Washington, to San Diego, California, along the western coast of the United States.

### Background

The MHP is a double-deck floating pier that rides with the tides. A typical pier is comprised of four modules 88 feet wide (beam) by 325 feet long by 29 feet deep. The main hull is constructed of post-tensioned, high strength, lightweight concrete with corrosion resistant steel reinforcement. This pier is secured by a series of mooring shafts extending from the sea bottom through mooring pools along the centerline of the pier (Figure 1). Details of the MHP are documented in Reference 1. A Test Bed is being fabricated at the dry dock facility at Concrete Technology Corp in Tacoma, Washington. This Test Bed, upon completion, will be transferred by wet tow to Naval Station San Diego, California, for a series of tests to observe material and structural design as well as hydrodynamic responses. The towing operation is expected to take about 3 weeks in the late summer. Even though seaways are relatively clam in the summer season, offshore weather stations report wave heights exceeding 10 feet from time to time and exceeding 20 feet occasionally. Since safe havens are out of reach from the transit route, the success of this ocean tow heavily depends on the inherent stability of the Test Bed.


Figure 1 Modular Hybrid Pier

### Hull Geometries of the Test Bed

The MHP Test Bed is a short segment of the pier with a reduced beam width. The Test Bed features two modules that are 50 feet wide by 50 feet long by 29 feet deep, and joined by post tensioning to a rigid unit 50 feet wide by 100 feet long (Figure 2). A service deck is located at 16.67 feet above the keel. The lower portion of the Test Bed up to the service deck consists of eight watertight compartments. A square mooring pool of 15 feet on each side is located on the centerline with its center situated at 20 feet from the stern of the Test Bed. The operation deck is 11.33 feet above the service deck. Both the bow and stern ends, above the service deck, are open.

Four utility windows are located on each side of the Test Bed with their lower edges 2.6 feet above the service deck. The Test Bed will be ballasted to an average draft of 13.5 feet with a small trim by the stern. Total displacement including the ballast weight is estimated to be 4.13 million pounds with its center of gravity at 14.35 feet above keel. For this platform to float in the described position, its center of gravity is estimated at 0.83 foot forward of midship.

Some unique features of the Test bed presented tough challenges to the stability analysis procedures. Factors that may influence the simulation strategy include its high center of gravity, low freeboard, large beam to draft ratio, and sharp corners. Despite the wide flat buoyancy hull, its heavy mass draws a deep draft and leaves a low freeboard to the service deck. Thus, the platform is very likely to take on green water as the service deck falters in and out of the water surface in heavy seas. Although this watertight platform can withstand severe deck immersion without flooding the buoyancy compartments, its wetted hull shape varies rapidly in heavy seas. This shape variation radically changes the transverse stability and restoring stiffness of the platform, and significantly complicates the surrounding fluid activities. The worst technical challenge comes from the extensive computation requirement of tracking the fluid forces in time, including both frequency-dependent hydrodynamic forces and the viscous damping taking place at the sharp corners. Water activity on the verge of capsizing is rather erratic and difficult to predict. Viscous damping, in addition to mitigating the motion response, may further change its phase angles relative to the ambient waves. The latter is of particular importance to the capsizing process and the ultimate stability of this platform in heavy seas. A qualified analysis tool must take these features into account.

However, heave changes the available freeboard and draft, which affects the maximum list angle the platform can tolerate without seriously altering its wetted hull geometry. Its phase angle relative to heel determines the shape of the wetted hull and the reserved stability of the platform. The wetted hull geometry also determines the fluid induced restoring stiffness, which affects the pace of platform responses. This time factor is, however, not included in traditional dynamic stability criteria.

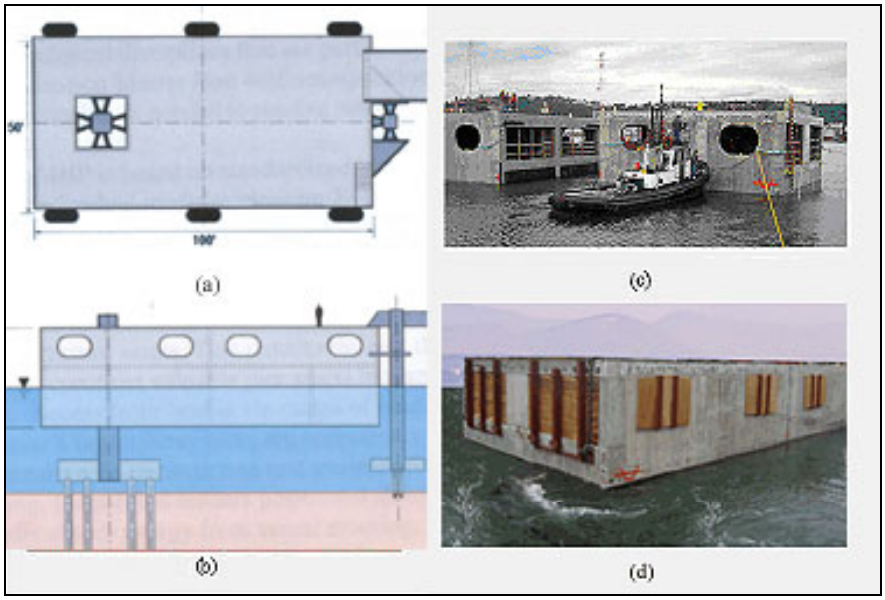


Figure 2. MHP Test Bed.

**Scope of Analysis**

Two configurations of the Test Bed were considered for the ocean tow. One retained the configuration as designed (Figure 2c) and the other had the entire space between the service and operation decks closed and sealed watertight (Figure 2d). The effective freeboard of the latter is quadrupled. These two candidate configurations will be referred as the open box (or Case a) and the closed box (or Case b), respectively. All floating compartments and enclosed spaces are assumed perfectly watertight.

Stability criteria are customarily divided into static criteria and dynamic criteria. All static criteria seek a minimum value of the metacentric height in an upright condition and all dynamic criteria attempt to define a threshold curve of static stability. However, curves of stability are normally generated in calm water without taking account of the wave effects and time factors. They are perhaps, no fair stability indicators for this low freeboard platform in heavy seas. Nevertheless, these curves summarize the hydrodynamic basics essential to the elucidation of a complicated capsizing process. This study started off with a complete description of the curves of static stability of the Test Bed, their sensitivity to the green water, and significance to the ultimate seaway stability. These curves are subsequently evaluated against the existing stability criteria to set a baseline for comparison with the succeeding dynamic analysis. The study then proceeded to establish a more reliable measure of the seaway thresholds for this low freeboard platform in terms of its seaway performance specified by a more sophisticated simulation code in time domain. Major tasks of the dynamic stability analysis include:

(a) Performance confirmation of the simulation model
(b) Quality check of the input waves used in the model
(c) Sensitivity test of the governing parameters
(d) Comprehensive assessment of the motion characteristics and the capsizing process
(e) Quantitative analysis of the platform response to seaways
(f) Final selection of the ultimate seaway stability.

The procedures and findings are documented in this report.

## STATIC STABILITY ANALYSIS

### Metacentric Height and Righting Arm

The metacenter (M) is the point around which the center of buoyancy (B) of a ship swings as the ship inclines slightly from its upright position. Consider a ship heeled a small angle to one side that causes the center of buoyancy to move off the centerline of the hull from B to B', as shown in Figure 3(a). The metacenter, M, is defined as the intersection between two vertical lines, one through the center of buoyancy of the hull in equilibrium (B), and the other through the center of buoyancy when the hull is inclined (B'). The location of metacenter of a ship varies with its displacement and trim. For a given draft and trim, this point remains practically stationary as the ship is inclined to a small angle up to 10 degrees, unless there is an abrupt change in hull shape in the vicinity of the waterline. As can be seen from Figure 3(a), the couple of ship displacement and buoyancy, separating by a righting arm GZ, forms a righting moment to counter ship movement. For a small angle of heel, this righting arm can be calculated readily with sufficient accuracy for practical purpose by the formula (Equation 1):

$$\overline{GZ} \approx \overline{GM} \bullet \sin\phi \tag{1}$$

The distance of GM is therefore an important stability indicator of a ship and is referred as the metacentric height. A ship is considered stable when this metacentric height is positive.

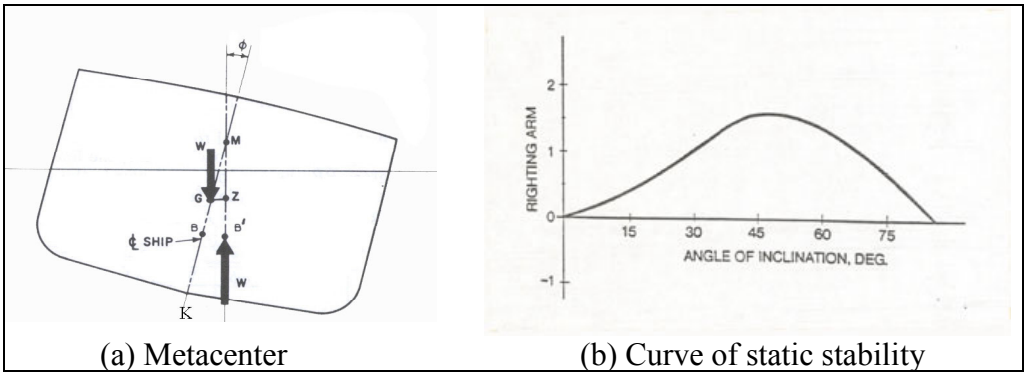


(a) Metacenter (b) Curve of static stability

Figure 3 Metacenter and Curve of static stability .

The location of metacenter is related to the geometry and draft of a ship hull by (Equation 2)

$$\overline{BM} = \frac{I}{\nabla}, \tag{2}$$

Where I is the second moment of inertia of the water plane area about its neutral axis in the associated mode of ship movement, and $\nabla$ is the volume of displacement. If the location of the center of gravity above the keel, KG, is known, the metacentric height, GM, can be readily determined by (Equation 3):

$$\overline{GM} = \overline{BM} + \overline{KB} - \overline{KG} \tag{3}$$

The location of the center of gravity, G, is normally determined by a standard inclining test as described in Appendix A.

The righting arm, GZ, varies as a ship heels away from its initial equilibrium attitude, and is conventionally presented as a curve of static stability in terms of heeling angle as shown in Figure 3(b). Naval architects use these curves to illustrate the stability character of a ship in general. At a small angle of inclination, sin φ may be approximated by φ in radians and the righting arm is thus reduced to (Equation 4):

$$\overline{GZ} \approx \overline{GM} \bullet \phi \quad \text{or} \quad \overline{GM} \approx \overline{GZ} / \phi \tag{4}$$

Thus, $\overline{GM}$ is signified by the gradient of the curve of stability at small angles of inclination.

The hull shape, displacement, and elevation of the center of gravity of a ship collectively determine the curve of stability. It should be noted that a large initial trim might substantially change the curves of stability for a low freeboard platform.

**Static Stability Curves for the MHP Test Bed**

A Fortran code Intact Stability Analysis Program, Version 4 (ISAP4) was used to generate the static stability curves for the Test Bed. This code tracks the equilibrium attitudes of the platform in calm water by balancing the static loads and buoyancy. The analysis procedure considers large angular motion and constantly updates the wetted hull geometries as the platform responded to external loads. This procedure automatically accounts for the effect of deck immersion. A static stability curve may be specified by correlating the equilibrium heel angles to a sequence of heeling moments. Details of the ISAP4 code, including the underlying theory, validations, analysis strategy, and program layouts are described in Reference 2.

The two candidate configurations of the Test Bed under consideration are modeled by equivalent boxes in the simulation as illustrated by Figure 4. The stability performance of both configurations in calm water is simulated with ISAP4 to observe the nature of the capsizing process. The results are presented in stability curves and movie animations.

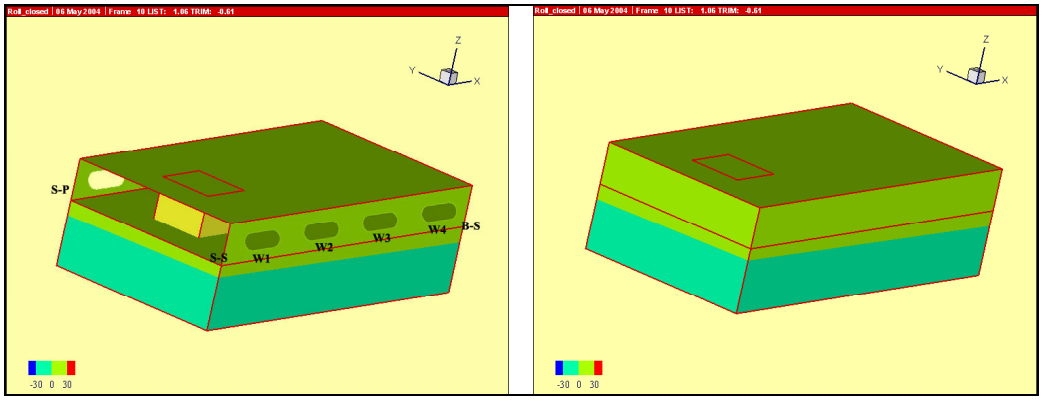


(a) Open Test Bed (b) Closed Test Bed

Figure 4. Alternative configurations of Test Bed for wet tow.

The curves of static stability for the Test Bed pontoon for both cases are presented in Figure 5. These curves were prepared using the best knowledge of the Test Bed modules to date. The hull geometry, displacement, center of gravity, mean draft, and desired trim were adopted or theoretically deduced from the design "bid set" drawings of 20 June 2003 (Reference 1). Highlights of the capsizing process are presented in Figure 6.

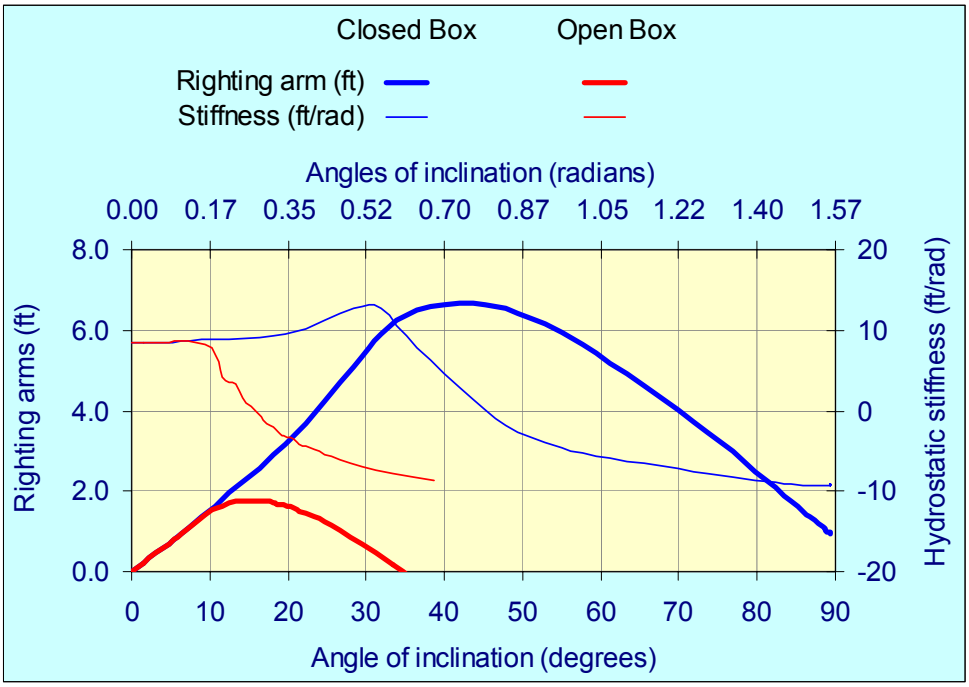


Figure 5. Curves of stability of MHP Test Bed.

It can be seen that the closed box is far more stable than the open box. The thin lines shown in Figure 6 are gradients (in ft/rad) derived from the corresponding stability curves. This parameter is an indicator of the hydrostatic stiffness of the platform. Its reading at a small angle of inclination is equal to the classical metacentric height of the platform, which is 8.2 feet in the present case. The platform is supported by buoyancy introduced through the wetted hull surface. Figure 6 (a) and (b) illustrates the wetted hull shape of the open and closed box, respectively, held by heeling moment at various attitudes.

Up to the angle of inclination of 8 degrees, both boxes experience the same hydrostatic resistance, because their water plane areas remain essentially no different. At this angle, the service deck just touches the water surface as shown in the second image of Figure 6 (a). Once the service deck dips into water, the open box rapidly loses its stiffness and its righting arm bends away from the initial stability. However, the righting arm continues to increase slowly and eventually reaches a peak of 1.8 feet at 15 degrees when the stiffness diminishes to zero, and then tapers off gradually toward zero at an angle of 34 degrees. The open box tends to flip over on its own weight beyond this point. This box in the attitude shown by the last image of Figure 6(a) will continue to roll and capsize. The righting arm of the closed box essentially follows the same pattern as that of the open box. However, its large freeboard pushes both the stability and the stiffness curves to levels much higher than those of the open box. The stiffness curve reaches the maximum at 30 degrees when the operation deck begins to dip into water and

rapidly decreases. The stability curve rises to a broad peak of 6.6 feet at the heel angle of 44 degrees before tapering off toward 90 degrees.

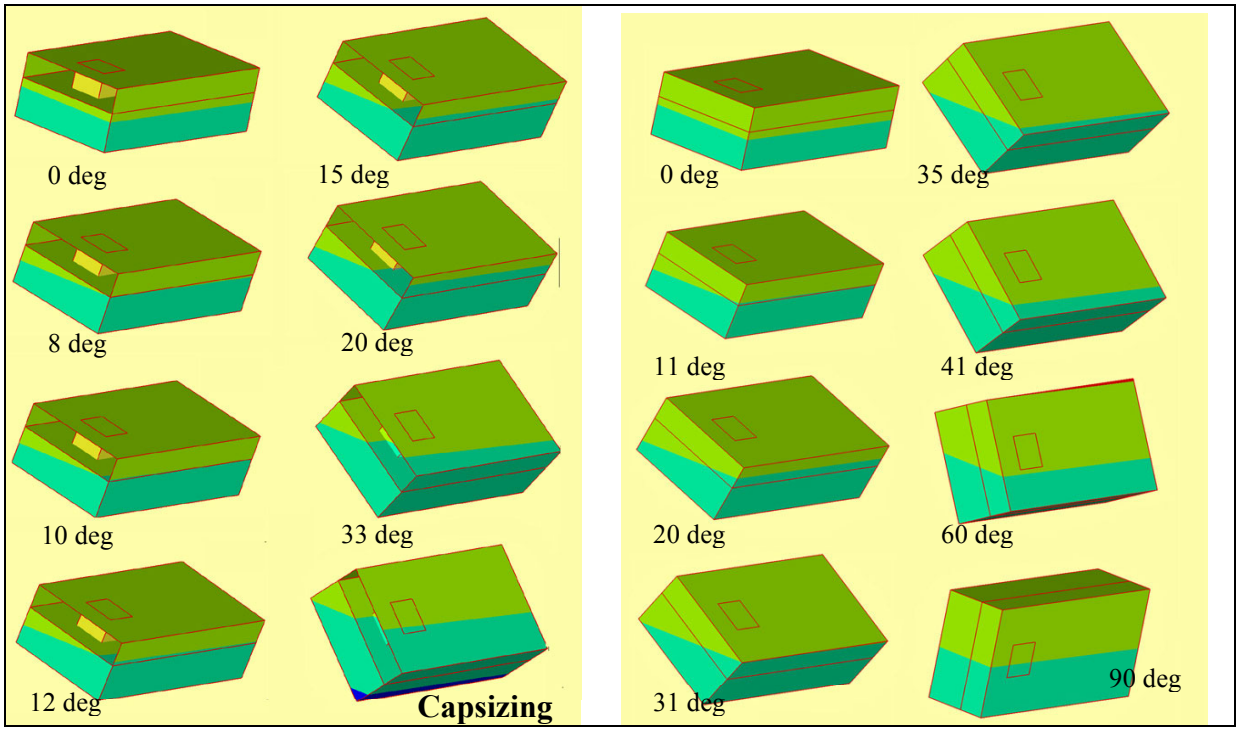


(a) Open Box (b) Closed Box

Figure 6. Stability graphics from animation.

**Static Stability Reduction Due to Waves**

The curve of static stability is the primary instrument to judging the transverse stability of a ship. It has been noted, however, that the actual righting moment of a heeled ship operating in a seaway may differ markedly from that predicted by the curve of static stability that is generated under an ideal condition in calm water. Paulling (Reference 3) showed that, under certain conditions, the stability of a ship might be reduced to an extent that jeopardizes its ability to withstand capsizing. He attributed the difference to two major sources: (a) the altered geometry of the immersed hull in waves, and (b) the altered pressure distribution over the hull in waves due to the wave induced fluid motion. He further indicated that this effect is of particular importance for ships with large beam-to-draft and low freeboard-to-beam ratios. Proper corrections are mandated to obtain the ultimate stability of such a ship in a seaway. Figure 7(a) was extracted from Reference 4 for small vessels under 100 meters in length. The trend of stability reduction due to wave influence seems in line with the prediction by Paulling.

A severe reduction in stability due to wave surfing in astern seas is unlikely to occur when the Test Bed is under tow at slow speeds. However, the test with a low freeboard-to-beam ratio can lose substantial water plane area due to severe pitch motion in rough seaways. Figure 7(b) demonstrates severe reductions in righting arms as the Test Bed floats at large trim angles.

At the trim angle of 6 degrees this platform, as designed, loses 50 percent of the static stability. It should not be a surprise that the Test Bed pitch exceeds this range in heavy seas.

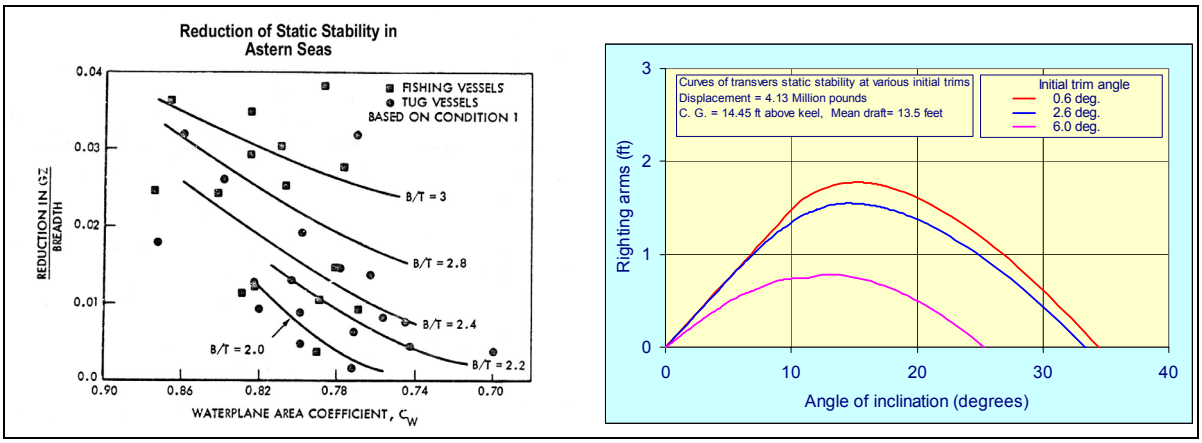


Figure 7(a). Reduction in GZ when perched on wave versus $C_W$ for towing and fishing vessels

Figure 7(b). Reduction iun transverse GZ of Test Bed due to trim angles.

The elevations of selected points above the water line including the mid points of the lower edges of windows on the starboard side (W1, W2, W3, and W4) and four corners of the service deck (S-S, B-S, S-P, and B-P) are presented in Figure 8. Locations of these eight points are illustrated in Figure 4(a). In the departure condition, the edge of the service deck begins to immerse at the stern as the Test Bed heels by 8 degrees and the bow by 10.5 degrees.

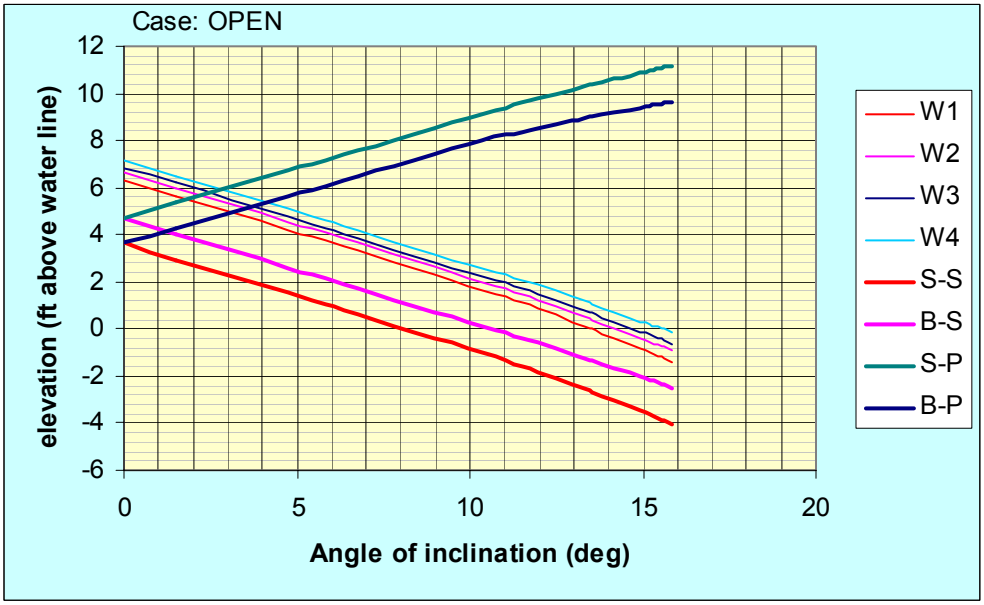


Figure 8. Elevations of selected locations at various angles of inclination.

**Stability Criteria**

The Navy and International Maritime Organization (IMO), each specified a general guideline for static stability assessment for their fleet.

The Navy adopted the Sarchin and Goldberg rule (Reference 5) as the base of stability criteria for Navy ships. This principle assumes a ship to heel to a 25-degree inclination to one side (or the knock down angle) and start bouncing back (as illustrated in Figure 9). At this time, the wind starts to bear on the ship hull and brings the ship back to the other side. The heeling energy imparted to the ship before the right moment equalizing the heeling moment at point c are by the restoring energy before ship hull exhausting the right moment. The Sarchin and Goldberg rule requires the righting energy to have a 40 percent reserve (i.e., the righting energy should be 40 percent greater than the heeling energy). It also requires that the heeling arm at the point equal to the righting arm should not be greater than 60 percent of the maximum GZ. The knock down heel angle of 25 degrees is an intuitive selection that most Navy ships do not exceed this limit.

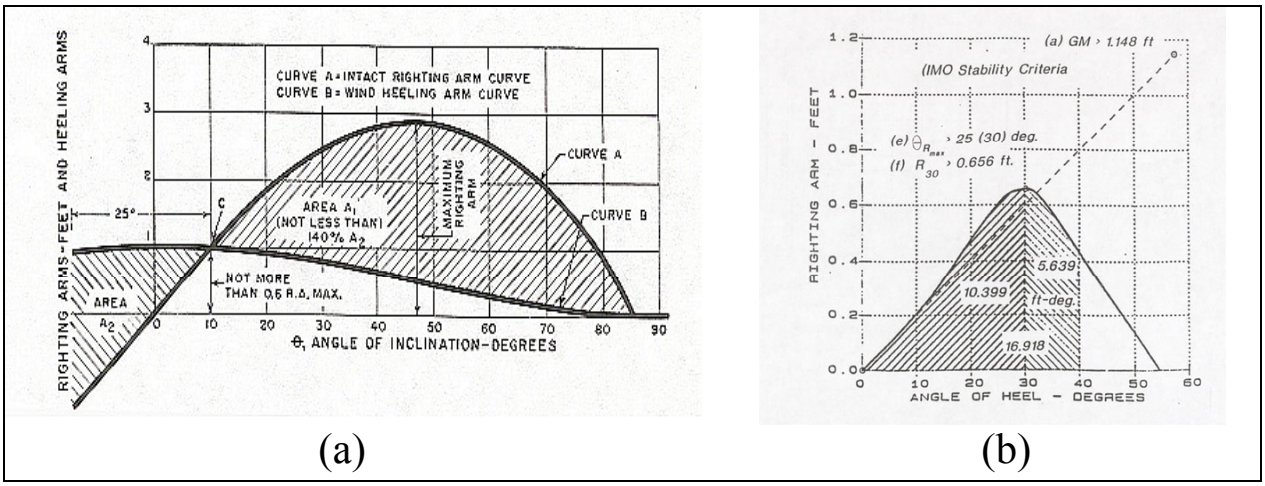


Figure 9. Stability criteria: (a) Sarchin-Goldberg, (b) IMO.

The Navy's standard practice recommends the following formula for the assessment of wind heeling arm (H. A.) (Equation 5).

$$\text{H.A.} = \frac{0.004\,V_w^2\,A\,\ell\cos^2\,\phi}{2240\,W} \tag{5}$$

Where:

$A$ = projected sail area, square feet

$\ell$ = lever arm, vertical separation distance from center of lateral water resistance to centroid of hull and superstructure lateral area, feet

$V_w$ = wind velocity, knots

$\phi$ = angle of inclination

$W$ = displacement in long tons

The Navy standard practice further specifies that 60 knots is the minimum wind velocity for design purposes of ships that will be recalled to protected anchorages if winds over Force 8 are expected. Other parameters pertinent to MHP Test Bed are:

$A$ = 1,500 square feet
$\ell$ = 14.5 feet
$V_w$ = 60 knots
W = 1,843 long tons

The heeling arm due to wind loads reduces to (Equation 6)

$$\text{H. A.} = 0.076 \cos^2 \phi \tag{6}$$

This result is plotted against the static stability as computed for the Test Bed in Figure 10. It is noted that the wind heel in this case is negligibly small in comparison to the available static stability. The wind heeling arm intersects the righting arm curve at 0.076 or 4.3 percent of its maximum. Apparently, this heavy platform of concrete construction is not sensitive to wind loads. Therefore, the stability of this platform therefore depends solely on the wave induced heeling. The requirement of 40 percent reserve stability will then limit the maximum heel angle of the open box to 20 degrees and the closed box to 60 degrees, respectively. Table 1 summarizes the results of static stability test against Navy criteria for ships. The closed box (Case (b)) fulfills both requirements of the wind heel criteria, whereas the open box (Case (a)) fails to provide sufficient restoring energy for the condition of 25-degree knockdown angle. As a result, Case (a) may not survive high sea states that heel the platform beyond 25 degrees.

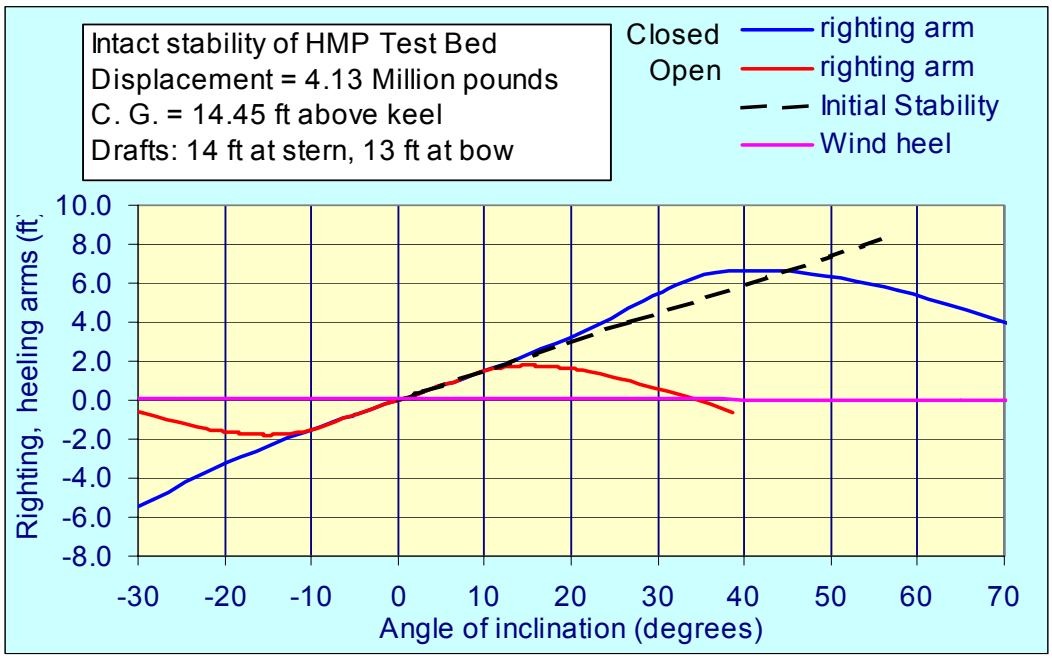


Figure 10. Static stability of Test Bed versus wind heel criteria.

Table 1. Test Bed Pontoon Stability Measured Against U.S. Navy Wind Heel Criteria

| Case | Knockdown angle (degrees) | Heeling energy (ft-deg) | Available Restoring energy (ft-deg) | Ratio | Required Ratio | Results |
|---|---|---|---|---|---|---|
| (a) Open | 10 | 8 | 37.3 | 4.7 | 1.4 | Pass |
| (a) Open | 25 | 31 | 37.3 | 1.2 | 1.4 | Fail |
| (b) Closed | 30 | 85 | 356 | 4.1 | 1.4 | Pass |
| (b) Closed | 50 | 200 | 356 | 1.8 | 1.4 | Pass |

The IMO provides the following recommendations for small ships (less than 100 meter) and fishing vessels as described in Reference 6 (Figure 9(b)).

- The area under the righting arm curve should not be less than 0.055 m-radian (10.34 foot-degrees) up to inclination angle of 30 degrees.
- The area under the righting arm curve should be not less than 0.09 m-radians up to 40 degrees or up to an angle where the non-weather tight opening come under water, whichever is less.
- The area under the righting arm curve between 30 and 40 degree (or down flooding angle) should be not less than 0.03 m-radian.
- The righting arm at 30 degrees or greater should be at least 0.2 meter
- The maximum righting arm should occur at an angle of inclination exceeding 30 degrees.
- The metacentric height GM should be not less than 0.35 meter.

Table 2 shows the comparison between Test Bed stability characteristics and IMO requirements for small ships and fishing vessels. Again, IMO criteria confirm the stability of the closed box and post a few warnings on the open box.

Table 2. Test Bed Characteristics Versus IMO Requirements for a Small Ship

| Parameters | IMO Criteria | Test Bed (Open) | | Test Bed (Closed) | |
|---|---|---|---|---|---|
| Range of positive stability | | 34 degrees | N/A | 90 degrees | N/A |
| Angle of maximum stability | > 30 degrees | 15 degrees | Fail | 44 degrees | Pass |
| Maximum stability | | 1.76 feet | N/A | 6.8 feet | N/A |
| Down flood angle (at bow) | | 10.6 degrees | N/A | 33 degrees | N/A |
| Down flood angle (at stern) | | 8.2 degrees | N/A | 31 degrees | N/A |
| Area up to 30 degrees | 10.34 ft-deg | 36 ft-deg | Pass | 76 ft-deg | Pass |
| Area up to 40 degrees or down flood angle | 16.91 ft-deg | 9.7 ft-deg | Fail | 147 ft-deg | Pass |
| Area between 30 degree and down flood angle | 5.6 ft-deg | 1.2 ft-deg | Fail | 280 ft-deg | Pass |
| Righting arm at 30 degrees | 0.66 feet | 0.6 feet | Fail. | 5.4 feet | Pass |
| Initial stability, GM | 1.15 feet | 8.4 feet | Pass | 8.4 feet | Pass |

**General Remarks on Stability Criteria**

Validity of safety criteria was endorsed by records of safe operations of vessels whose stability parameters comply with those criteria. Both the Navy's wind line criteria and IMO criteria show tractable records of guiding the implementation of adequate stability characteristics to their fleets. However, statistics are not sufficient to demonstrate the credibility of any criteria full protection of small vessels in all waters and in all weathers. Uncertainties can be shown by many documented casualties:

(1) Small fishing boasts were lost when operating in light condition
(2) A North Sea coaster was lost in a light condition
(3) The loss of a new British stern trawler with all hands aboard in the winter of 1973 to 1974, in the North Sea
(4) The similar disappearance of several crab boats in 1975 in western Alaskan waters.

The term "dynamic" in the traditional stability criteria is somewhat misleading for the reason that the time factor is not included in the analysis. Stability (GZ) curves are assessed in calm water and do not include wave effects. It is well known that the static stability of a ship changes in time as the ship moves in seaways. Curves of static stability show, at most, the threshold heel angle when positive stability diminishes. However, they do not predict when and how a ship reaches the threshold heel angle nor do they correlate ship dynamics to the true static stability of the ship at that angle. Consequently, static stability criteria are often used as a general guideline rather than a complete evaluation tool.

The ultimate stability of the platform in seaway should be further assessed by dynamic simulation on a rational basis. This process offers the chance to introduce the crucial time factors into the assessment process.

## DYNAMIC STABILITY ANALYSIS

Seaway performance of a ship determines its ultimate stability for a specific operation. This flat platform, of low freeboard, is prone to heavy green water hence; it constantly changes its wetted hull shape while underway. This greatly complicates the surrounding fluid activities, thus, imposing a stiff challenge to the simulation technique. Simulation codes, capable of tracking the rapidly changing wetted hull geometry and fluid forces in time, are required for full protection of the platform. A high-resolution computational fluid dynamic (CFD) code is available, however, the intensive computational obligation is beyond what the present project can afford. This study adopts a potential theory based, time domain code, MULTISIM, as a cost-effective alternative. This code was originated by Paulling (Reference 7) for the Navy in support of the conceptual development of a deck barge similar to the Test Bed. An extensive parametric study was initially conducted to confirm the performance of this code and explore the sensitivity of the dominating parameters. Findings were used to select a realistic numerical model best representing the ocean tow scenario. The code and numerical model were then used to explore the capsizing process and determine the threshold seaways that the Test Bed can possibly withstand during the forthcoming ocean tow. However, it should be noted that this threshold only protects the Test Bed against wind waves. Casualties due to unusual seaways or operations cannot be ruled out.

### Hydrodynamic Characteristics of the MHP Test Bed

The hydrodynamic character of this platform is inspected in mild seaways with several frequency domain codes and the MULTISIM code. The results provide a reference to the subsequent performance assessment of the Test Bed in high sea states. These simulation codes and associated findings are briefly summarized as follows:

SMP, CATMO, and HYDRO3**.** The SMP (Ship Motion Program) code (Reference 8) of the Navy is a potential theory code, based on the early "strip theory," for general seaway performance of the U. S. military fleets. CATMO (Causeway Train Motion) code (Reference 9) adopts the hydrodynamic feature from the original SMP code of 1971. This code was further fine tuned for small deck barges of rectangular hull shape. HYDRO3 is a potential theory code authored by Hong and Paulling (Reference 10). All three codes assume that the motion of the body consists of a small oscillation about a stationary mean position and properties of the fluid flow are determined by the flow theory based on the irrotational and inviscid fluid.

CATMO predicted a significant roll amplitude of 10 degrees in beam waves of Sea State 7 as shown in Table 3. This is less than the upper boundary of positive stability of 15 degrees for the open box, and 34 degrees for the closed box. However, this code addresses seaways with Pierson-Moskowitz spectra, in which the peak period is correlated to the wave height for a specific Sea State. The peak period for Sea State 7 is much longer than that of the natural roll period of MHP Test Bed. This platform would have rolled substantially more than 10 degrees in Sea State 7 if the peak period were shorter.

Figure 11 highlights the Test Bed performance predicted by HYDRO3 in terms of the response amplitude operators (RAO). The motion RAOs predicted by SMP in beam seas are also presented in discrete circles for comparison. These two codes predict essentially the same results in beam seas. Both indicate that the Test Bed is most sensitive to waves within the frequency

window between 0.1 and 0.2 hertz, or the equivalent wave period window between 5 and 10 seconds. Outside this window, the Test Bed either rides on the long waves or is insensitive to the short waves.

MULTISIM Code. MULTISIM is intended for analysis of the dynamic response of a multi-module floating platform to disturbances due to waves, wind, and current. The program treats a platform that is made up of connected floating modules. Each module consists of a body of arbitrary shape. The modules may be linked to one another and/or anchored to the seafloor. The external forces acting on the platform consist of those due to wave, platform motion, and the position keeping system. For platforms of large beam to depth ratio, the principal external force is the Froude-Krylov or dynamic buoyancy force. This component is computed for the exact instantaneous position of the body relative to the wave surface. The remainder of the force, consisting of frequency-dependent wave diffraction and radiation forces, is computed by an approximation based on small wave and motion amplitudes. These frequency-dependent forces have to be computed by means external to MULTISIM.

In order to include the frequency-dependent components in a time domain solution scheme, it is first necessary to compute time dependent impulse response or "memory" functions by taking the Fourier transform of the frequency-dependent force transfer functions. A time history of the force is then obtained by means of a convolution integral of this memory function over the motion time history.

The computation of the total fluid force is a hybrid process combining the small amplitude, frequency-dependent potential flow effects with large amplitude, real fluid effects. Both the Froude-Krylov and Morison formula forces are evaluated over the instantaneous immersed position of each module or cylindrical member at each time step and are exact within the respective framework for large wave and motion amplitude. However, the potential flow effects are based on small amplitude theory and are strictly valid only in the case of waves and motions that is within the limits of the theory.

The analysis procedure used by MULTISIM is based on a time-domain numerical integration of the platform's rigid-body equations of motion, taking into account the exact large amplitude motion effects. This time domain solution permits typical nonlinear effects to be treated, including forces due to fluid drag, finite amplitude wave and ship motion, and anchoring or position keeping systems.

Fluid drag due to viscosity is not directly addressed in the potential theory-based simulation models including the MULTISIM code. Compensation is normally made through a parametric model based on a Morrison equation that includes empirical coefficients. In this approach, viscosity damping is approximated by the equivalent fluid drags experienced by circular cylinders of negligible diameter attached along the sharp edges of the flat keel as the Test Bed scrapes through the ambient water. The drag force is proportional to the relative velocity squared and all other parameters including fluid density, viscosity, and cylinder size are lumped into a single equivalent drag coefficient. The required drag coefficients for the Test Bed will be determined by field tests upon completion of the Test Bed construction.

Table 3. Roll Amplitude Predicted by CATMO

| Sea State | Significant wave amplitudes | Period at the maximum energy | Significant roll amplitudes |
|---|---|---|---|
| | (feet) | (seconds) | (degrees) |
| 5 | 12 | 9.6 | 6 |
| 6 | 18 | 11.7 | 8 |
| 7 | 30 | 15.1 | 10 |

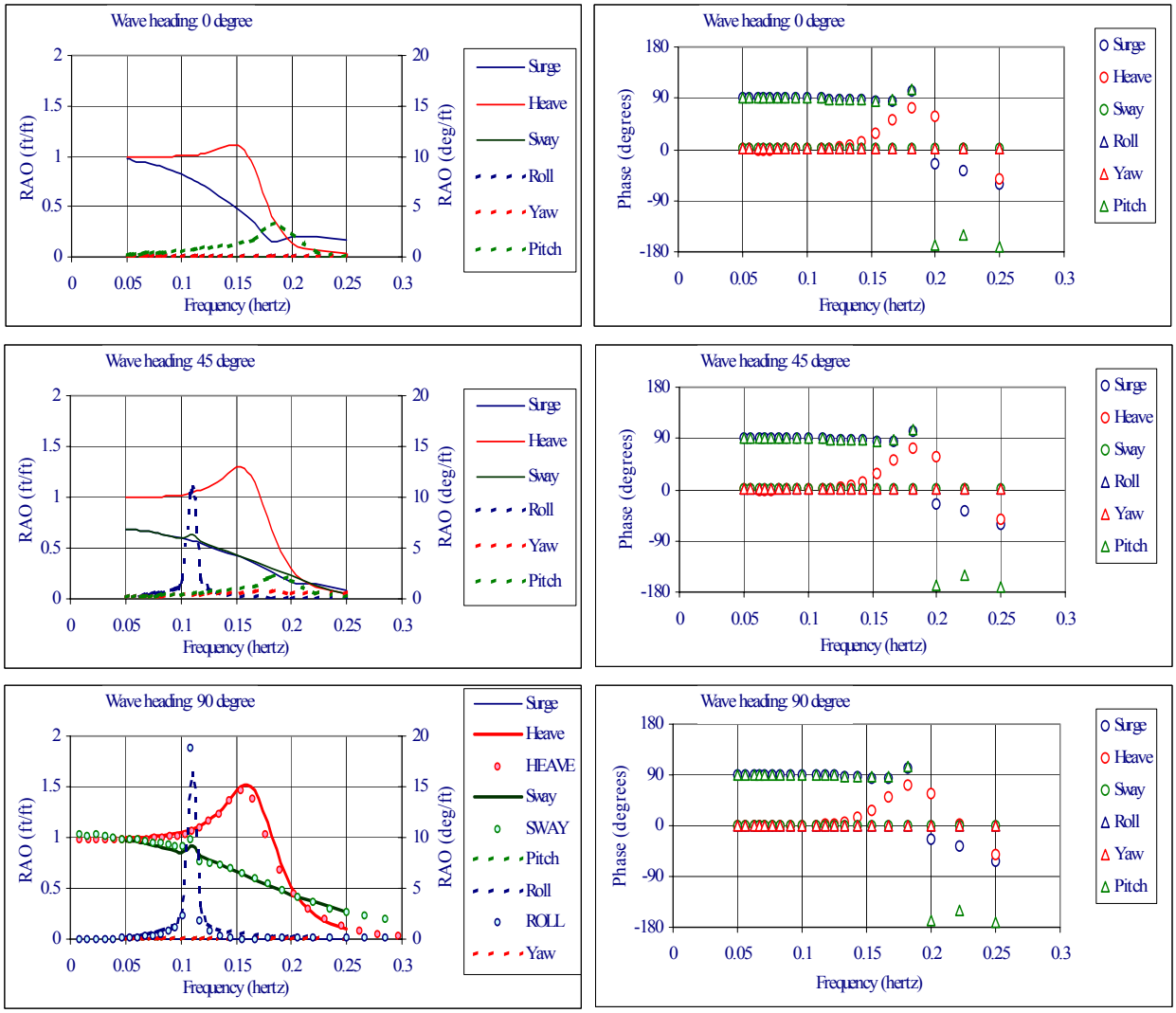


Figure 11. Test Bed responses predicted by linear potential theory code, HYDRO3 (lines), and SMP (circles).

**Numerical Model of MHP Test Bed**

This effort focuses on the seaway performance of the Test Bed under ocean tow. A parallel analysis is conducted to address the couplings between tug and tow as well as the resulting towline dynamics en route. The results are presented in Reference 11. This analysis predicted a tug thrust requirement of 14 kips and a maximum hawser load of 23 kips. Both are negligibly small in comparison to the wave forces and therefore neglected from the subsequent dynamic analysis. It has been determined in the static stability analysis that the designed wind heeling is only 4 percent of the maximum restoring capacity of the open box. The 15- by 15-foot mooring well is also neglected to simplify the fluid activities associated with the capsizing process. The area of this opening is less than 5 percent of the total water plane of the platform and is located at the centerline of the platform. Therefore, its contribution to the roll restoring arm is limited. As a result, a rectangular box of the same envelope as that of the Test Bed up to the service deck (i.e., 100 feet long by 50 feet wide by 17.67 feet high) is chosen to represent the open box. Similarly a box 29 feet tall is chosen to represent the closed box. The shorter box is used for the computation of frequency dependent parameters. The mass distribution, the mean draft, and the initial attitude are identical for both cases. Table 4 summarizes the particulars of the model platforms used in the present simulations. The platform is lightly moored in the numerical simulation against wave-induced drift (Figure 12). Four soft mooring lines, roughly 5,000 feet long, extending symmetrically about the principal axis of the platform on the horizontal plane through its center of gravity, are used to hold the platform in equilibrium at the beginning. These lines are attached to the platform at the ends along the centerline. This layout is intended to maintain the vertical angles of the mooring lines within a fraction of 1 degree as the platform heaves in severe Sea States and thus minimize their contributions to the heeling moment. Otherwise, the platform is expected to respond to waves freely.

Two coordinate systems are used to describe the platform performance as illustrated in Figure 12. One is a body fixed coordinate, OXYZ, located at the center of gravity of the platform, with its X-Z plane parallel to the mean water surface when the platform floats at rest in calm water. The positive X-axis points toward the stern and the positive y-axis points upward to complete a right hand coordinate system. The second coordinate system, oxyz, is fixed in space and initially coincides with the body fixed system, serving as an inertial reference. The motion of the Test Bed is described by the three translational excursions of the center of gravity in x-, y-, and z- directions from its initial position and a set of three Euler angles defined as follows. The platform first rotates about its initial OY axis through a yaw angle, $\theta_2$, then rotates about the new OZ axis through a pitch angle, $\theta_3$, and finally rotates about the resulting OX axis through a roll angle, $\theta_1$. The wave heading is measured clockwise from the ox axis.

For the evaluation of the fluid induced forces, the wetted hull surface of the Test Bed models was digitized into triangular patches as shown in Figure 13. The nodes may be specified in any reference of convenience provided that its origin is properly referred to in the global system. For the purpose of capsizing analysis, the entire exterior surface of the buoyancy hull is digitized. The particulars of the model platform used for the present simulation are summarized in Table 4.

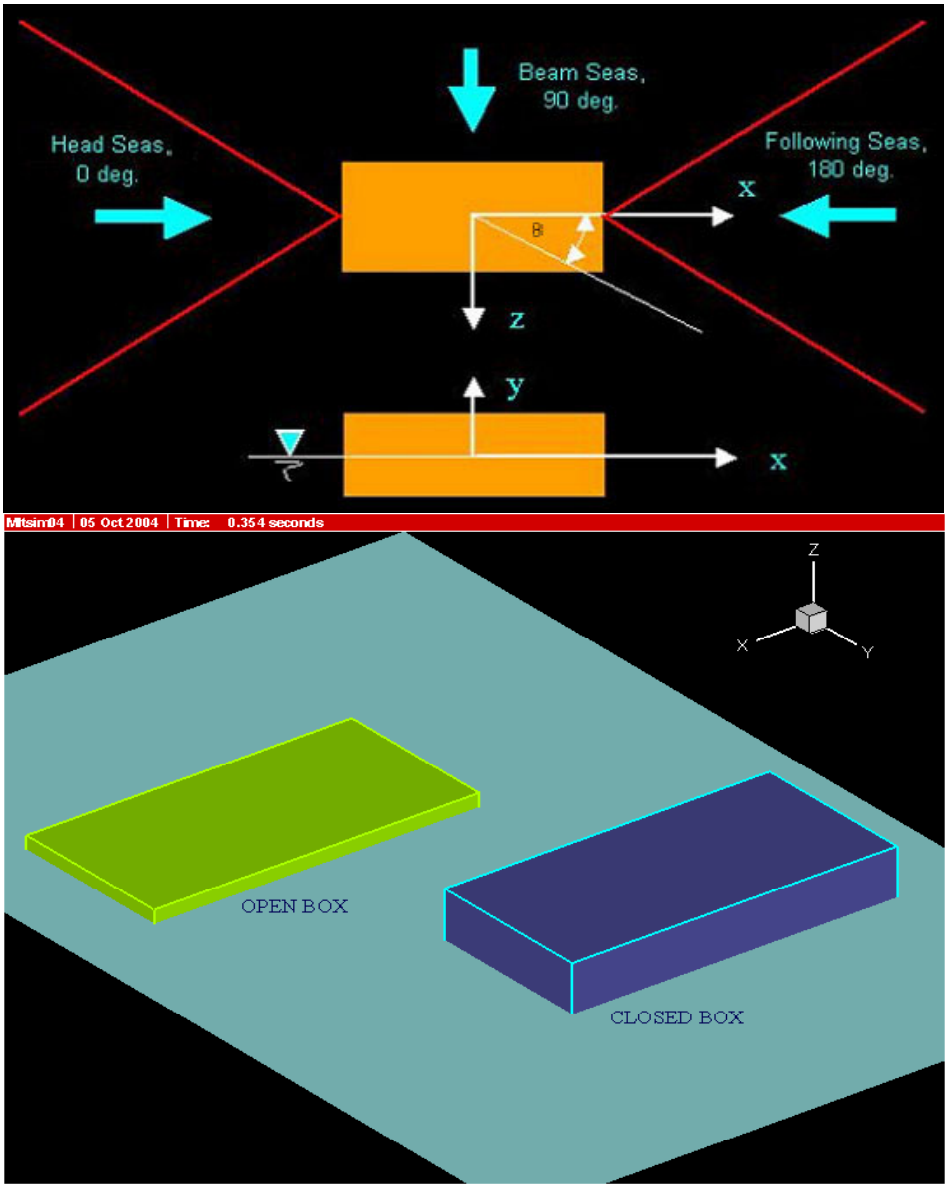


Figure 12. General layout of the numerical model for capsize analysis.

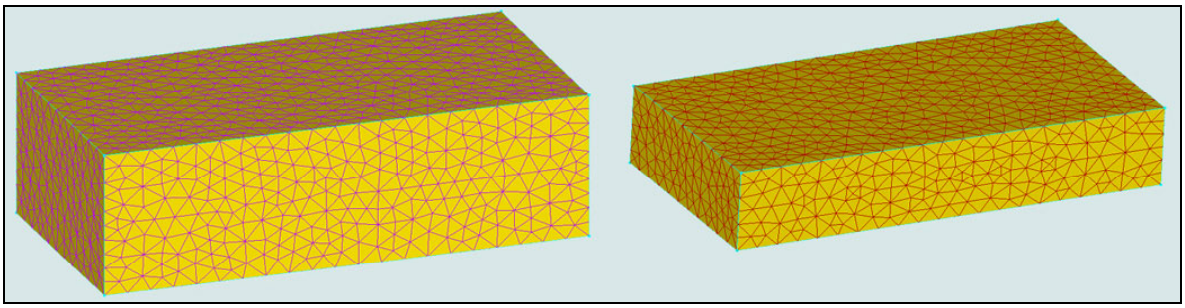

(a) Closed Box (b)Open Box

Figure 13. Numerical digitization of Test Bed for MULTISIM Code.

Table 4. Test Bed Particulars

| | Parameters | Values |
|---|---|---|
| **Dimensions** | Length | 100 feet |
| | Beam | 50 feet |
| | Depth | 29 feet |
| | Mean Draft | 13.5 feet |
| **Mean Freeboard** | Open box | 3.17 feet |
| | Closed box | 15.5 feet |
| **Mass Properties** | Displacement | 4,130,000 lbs |
| | Gyradius, x | 14.43 feet |
| | Gyradius, y | 28.87 feet |
| | Gyradius, z | 28.87 feet |
| **Center of Gravity** | Longitudinal | Midship |
| | Elevation above keel (y) | 14.35 feet |
| | Lateral (z) | Center line |
| **Initial stability** | GM | 8.2 feet |
| **Equivalent Viscous Damping Coefficients** | Roll | 400 |
| | Pitch | 400 |

**Characteristics of Input Waves**

Since the wind heel moment associated with the design storm of 60 knots is relatively small, ocean waves are the primary environmental force for the consideration of stability against capsizing. The present ocean tow calls for a survival wave criteria of Sea State 6. The numerical simulation walks through the range from Sea State 3 to Sea State 7 in order to identify the seaway thresholds for the towing operation. Both regular swells and random seas are included. No directional spreading is considered.

Swells. Swells are waves propagating far outside the wind sources. They appear in a fairly smooth profile with a clear dominating period and heading. They are normally represented mathematically by sinusoidal functions. More than one swell system may exist concurrently at a site. MULTISIM treats multiple swells with a linear sum of their associated sine functions. The water elevation $\eta$ at a location x and time t is represented by (Equation 7):

$$\eta(x,t) = \sum_{i=1}^{n} a_i \cos(k_i x - \omega_i t - \varepsilon_i) \tag{7}$$

Where:

$a_i$ = wave amplitude,
$\omega_i$ = wave frequency in rad/sec,
$k_i$ = wave number = $2\pi/\lambda$,
$\varepsilon_i$ = wave phase.

The fluid is assumed inviscid and flow irrotational such that a velocity potential, $\phi$, exists. The wave motion of i-th component can be thus given for water depth d by (Equation 8)

$$\phi_i(x,y,t) = \frac{ga_i}{\omega_i} e^{k_i x} \sin(k_i x - \omega_i t - \varepsilon_i) \quad (8)$$

The associated pressure, water elevation, and water particle kinematics are the linear derivatives of this velocity potential and the following dispersion relationship between frequency ω (rad/sec) and wave number, k, holds (Equation 9):

$$\omega^2 = gk \tanh(kd) \quad (9)$$

Random Seas. Waves within or just leaving a storm appear highly irregular and unpredictable. They are normally described by statistical models in terms of their energy content. A widely accepted wave model assumes that an irregular seaway is a narrow banded Gaussian process. The bell shaped Gaussian function best describes the water elevation distribution at a certain location. This assumption in turn leads to the well-known Rayleigh distribution model of the associated wave heights. Field measurements in open water around the world unanimously concur with this theoretical model. Within this model, the variability of wave height and wave period can be closely approximated by the following distribution functions.

Wave Height Distribution

$$f(H) = \frac{H}{4m_o} \exp(-\frac{H^2}{8m_o}),$$

Where $m_o$ is the total energy of the wave system. Based on this wave model, a random wave field can be represented by concise wave height statistics. The most popular parameter for engineering practice is the significant height, $H_s$, or the averaged height of the highest one third of all waves. The other parameters are related to this wave height by (Equation 10):

$$\begin{aligned} H_{\frac{1}{20}} &= 1.403\, H_s \\ H_{\frac{1}{10}} &= 1.271\, H_s \\ H_{\frac{1}{5}} &= 1.124\, H_s \end{aligned} \quad (10)$$

The most probable maximum height, $H_{max}$, in a wave sequence over a period of time is related to $H_s$ by (Equation 11):

$$H_{\max} = 0.707 H_s \sqrt{\ln N} \quad (11)$$

Where $N$ is the number of consecutive waves. For a persistent wind system with the number of waves exceeding 1,000, the maximum wave height may reach 1.86 $H_s$.

In engineering practice, it is often assumed that structure responses induced by such wave systems inherits the same statistical nature such that these correlation coefficients may also apply.

Wave Period Distribution. Bretschneider proposed based on field measurements that the wave lengths of wind generated seas are also Rayleigh distributed. This assumption leads to the following wave period distribution (Equation 12):

$$f(\tau) = 2.7\ \tau^3\ \exp(-0.675\ \tau^4) \tag{12}$$

Where $\tau = \frac{T}{\overline{T}}$, $\overline{T}$ denotes the mean value of wave periods.

Bretschneider Two Parameter Spectra. A Sea State is most frequently described through energy spectrum. Sufficient field evidence proves that wind generated wave spectra exhibits certain stable shapes. Two conventional model spectra of universal recognition are the Pierson and Moskowitz spectrum and the Bretschneider spectrum. Although slight differences between the two exist at early stages of wave generation, the spectra are essentially identical for fully developed seas. The MULTISIM code approximates random seas with irregular wave sequences converted from Bretschneider two parameter spectra along with uniformly distributed random phases. These spectra may be described in terms of significant wave height ($H_s$) and peak frequency ($f_o$) by Equation 13:

$$S(f) = 5\left(\frac{H_s}{4}\right)^2 f_o^{-1} \left(\frac{f}{f_o}\right)^{-5} e^{-\frac{5}{4}\left(\frac{f}{f_o}\right)^{-4}} \tag{13}$$

Figure 14(a) demonstrates some Bretchneider two parameter spectra used in the present analysis. Also presented in Figure 14 in discrete circular symbols is a spectrum deduced from the irregular wave sequence generated by MULTISIM code. The result is close in agreement with the target Sea State of 12-foot significant wave height and 7.5-second period at the peak energy, as illustrated. The key parameters, Hs and $f_{0,}$ are functions of wind field parameters and the stage of wind wave generation process. Figure 14(b) shows a set of Bretschneider spectra that are best fitted to the wave measurements observed during Hurricane Eloise of 1975. These measurements indicate that the two spectral parameters of realistic seaways are highly correlated, rather than being a pair of independent variables, as Equation 13 suggests. In general, the peak frequency, $f_o$, decreases as a wave system grows. However, fetch or duration limited storms may cause a moderate shift of the peak frequency, $f_0$. Two Bretschneider spectra of the same energy level, but of different peak frequency, $f_{0,}$, present different spectral shape as illustrated in Figure 14(a) by the two wave systems of 12 foot high. Bretschneider's two parameter spectra retain the flexibility to explore the impact of frequency variation. Figure 15 illustrates the variability of random waves generated in MULTISIM code. The resulting wave profile, height, and period distributions are almost identical to the field data justified theoretical distribution functions represented by the solid lines. The model seaway implemented in the MULTISIM code is therefore considered realistic.

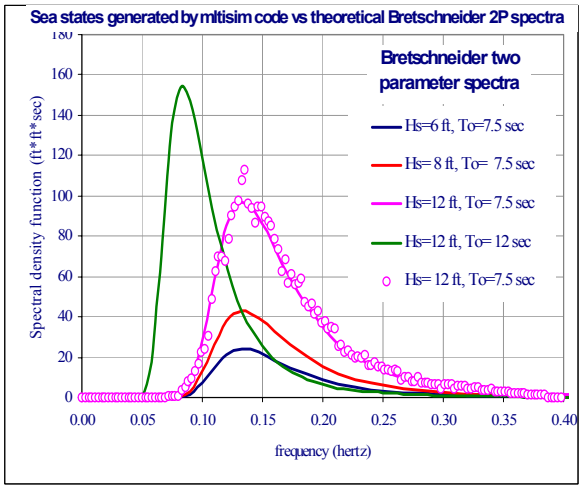


Figure 14a. Spectrum converted from wave arrays generated by the MULTISIM Code.

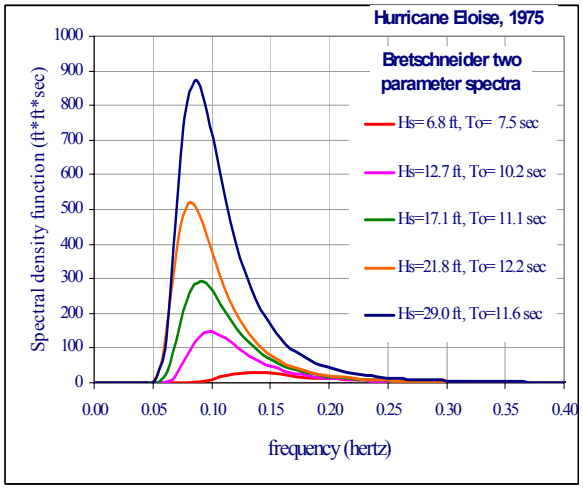


Figure 14b. Bretschneider spectra best-fit to waves observed during Hurricane Eloise.

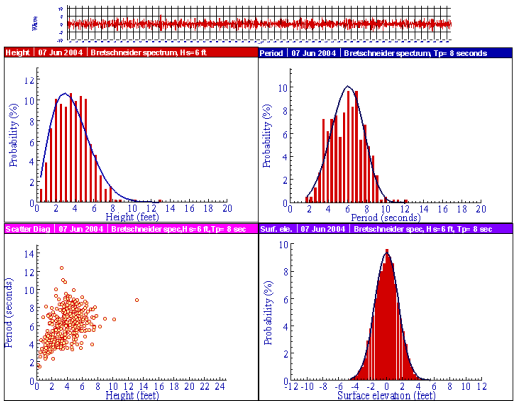

(a) Hs= 6 feet, $T_0$ = 8 seconds

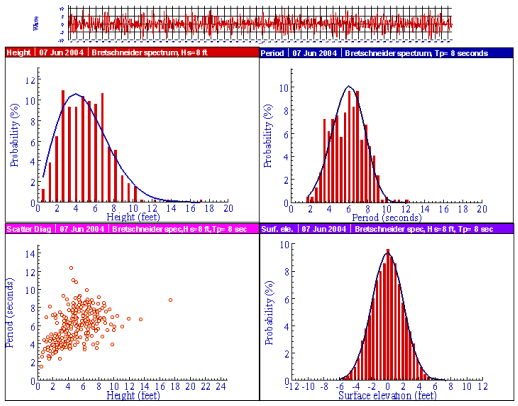

(b) Hs= 8 feet, $T_0$ = 8 seconds

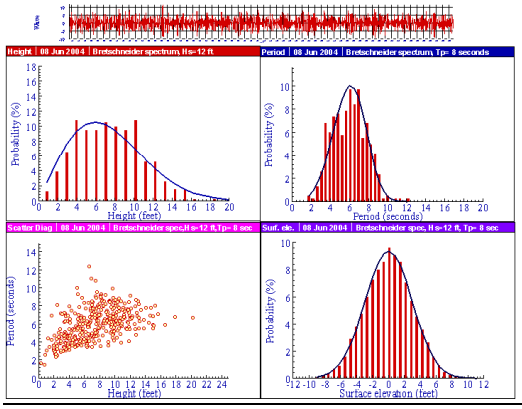

(c) Hs= 12 feet, $T_0$= 8 seconds

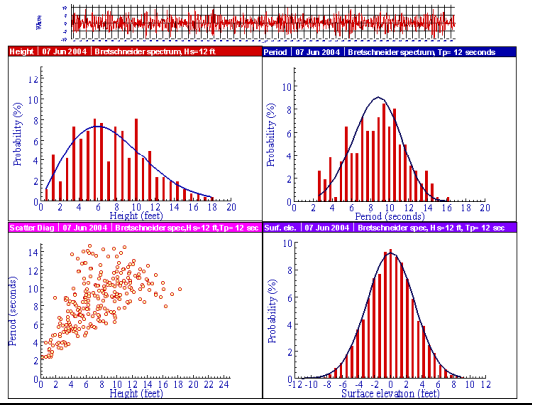

(d) Hs=12 feet, $T_0$=12 seconds

Figure 15. Variability of wave parameters.

**Sensitivity of the Governing Parameters**

A preliminary study was conducted to initially confirm the performance of MULTISIM code, explore the sensitivity and quality of the governing parameters, and thus establish a realistic numerical model best representing the actual ocean tow scenario. Wave period is perhaps the most critical parameter and its impact will be explored in great detail in the core analysis. Other dynamic parameters, including viscous damping coefficients, wave heights, elevation of the center of gravity, and mooring characteristics, will be tested for their sensitivity. Results are compiled to assist the design of the numerical model for capsizing analysis.

Mooring Stiffness**.** The mooring system implemented in the numerical model is to prevent the Test Bed from drifting out of its course under tow. However, this mooring system should not alter the high frequency motion of the Test Bed, or trip it in any way. This test series was conducted in quartering seas (45 degree) to better represent barge response in general. A random seaway of 6 feet high and 8-second peak period was used. While the mooring configuration remains identical, the line stiffness varied from 5 lbs/ft and 1,000 to 4,000 pounds per linear foot. It can be seen that with essentially no restriction at 5 lbs/ft, the Test Bed rapidly drifted out of the range and spun around. This behavior is not consistent with the condition with which the frequency dependent components of hydrodynamic forces were calculated, with the barge in its initial position and orientation. Consequently, some constraint is required for the simulation results to make sense. Figure 16 presents the results from this test series. It indicates that motions in the three modes with fluid restoring forces (i.e., heave, roll, and pitch) are almost identical as the mooring line stiffness increased from 1,000 to 4,000 pounds per linear foot. A stiffer mooring system only reduces the range of oscillations of the other three modes with no fluid restoring force. Consequently, a soft mooring system with a line stiffness of 1,000 pounds per linear foot is recommended to allow the Test Bed to sway over a range comparable to the anticipated fishtailing of the Test Bed under tow. This mooring system performs most favorably with mooring lines attached to the ends of the platform along its centerline at the elevation of its center of gravity.


Figure 16. Influence of mooring lines to the motion responses of Test Bed.

Viscous Damping. Viscous damping is crucial to the roll motion in light of a relatively weak wave radiation damping in this mode. This effect is more critical to the present simulation for two reasons: (a) the sharp edges of this hull are more likely to induce strong viscous damping, and (b) viscous damping increases quadratically with the relative current velocity, which will be much more pronounced in high sea states. Unfortunately, viscous damping is not directly addressed in the potential theory based simulation models. MULTISIM code introduces this essential correction through a parametric model of Morrison equation type that involves a empirical coefficient. It is assumed that fluid viscosity induced resistance may be approximated by equivalent drag forces imposed on a set of imaginary cylinders along the sharp edges of the platform as shown by Equation 14.

$$F_d = \sum C_D \frac{\rho}{2} D V_r \mid V_r \mid \delta\ell = \sum C_d V_r \mid V_r \mid \delta\ell \qquad (14)$$

Where D and $\delta\ell$ are the diameter incremental length of the cylinder, $V_r$ is the relative velocity of the cylinder with respect to the ambient fluid, $\rho$ is the specific gravity of the fluid, while $C_d$ and $C_D$ are quadratic drag coefficients. The force summation applies through the length of a cylinder. Since these cylinders do not exist, their diameters are set to a small size to avoid adding excessive buoyancy to the model platform and lumped into an equivalent drag coefficient ($C_{d)}$ along with the specific gravity ($\rho$). The magnitude of the drag force is thus control solely by the drag coefficient ($C_{d)}$. This coefficient is normally hull dependent and can only be determined experimentally. The required coefficients for Test Bed are not available at this moment. A sequence of test runs was conducted to observe the sensitivity of the damping coefficient to the motion results. This test was done in head seas. However, for the Test Bed with a beam to length ratio of 0.5, the effects are similar. Figure 17 illustrates the impact of viscous damping with the coefficients ($C_d$) increasing from 0 to 400 $lb \bullet sec^2/ft^3$. The viscous damping obviously affects pitch motion more than heave motion. This is, however, not a surprise as the heave motion normally induces higher radiation wave damping and therefore, is less influenced by the additional viscous damping. Motion results with damping coefficients in the range of 200 to 400 $lb \bullet sec^2/ft^3$ seem reasonable. A damping coefficient of 400 $lb \bullet sec^2/ft^3$ is able to bring the maximum roll RAO down to a realistic level of 2.5 deg/ft as shown in Figure 18.

Free decay is a simple and well-understood process and is thus frequently used to calibrate a simulation code and numerical model. This series of tests was conducted in calm water. The model Test Bed was set to an initial offset of five units (feet or degrees) in a specific mode from its static equilibrium position before being released to free oscillation. The platform then oscillated in its natural frequency with its amplitude decreasing at a rate dictated by wave radiation and fluid viscosity damping. The wave radiation damping is deduced from a set of frequency dependant hydrodynamic coefficients prescribed by an external source, whereas the viscosity damping is determined by a Morrison equation controlled by empirical coefficients. An arbitrary viscous damping coefficient of Cd=400 $lb \bullet sec^2/ft^3$ was selected for the present test runs. The results, as captured in Figure 19, look reasonable for a moderately damped oscillatory system. Motion in the three modes with restoring forces (i.e., heave, roll, and pitch) presents high resonant frequencies as shown in Table 5. The low frequency oscillations in the other three modes basically reflect a soft mooring system used in the present numerical model.

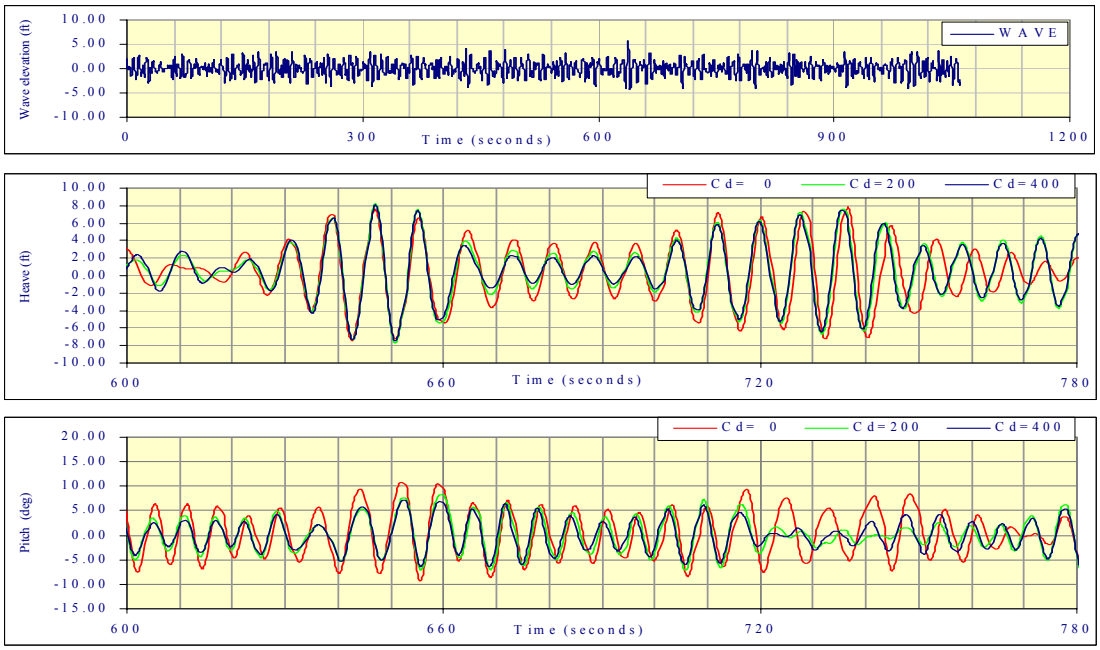


Figure 17. Influence of viscous damping on motion responses of Test Bed.

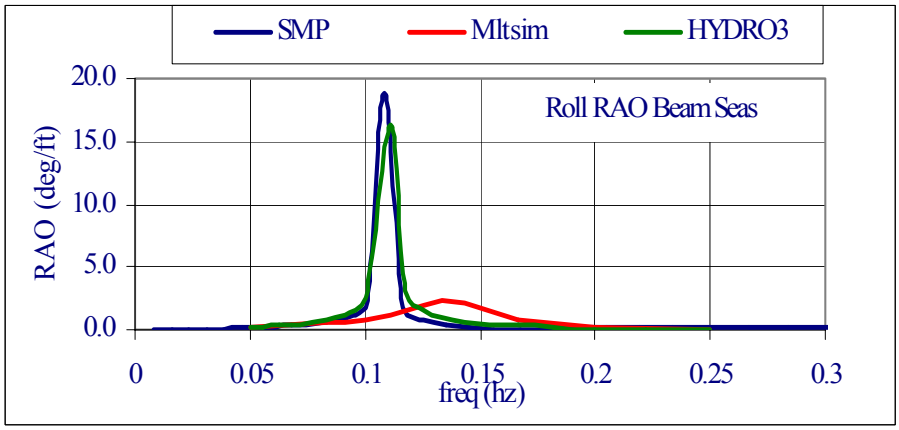


Figure 18. Influence of viscous damping on roll RAO.

Table 5. Natural Period of Test Bed Model

| Mode of motion | Natural Periods (seconds) | Mode of motion | Natural Periods (seconds) |
|---|---|---|---|
| **Surge** | 60. | Roll | 7.3 |
| **Sway** | 75. | Pitch | 6.2 |
| **Heave** | 7.5 | Yaw | 35. |

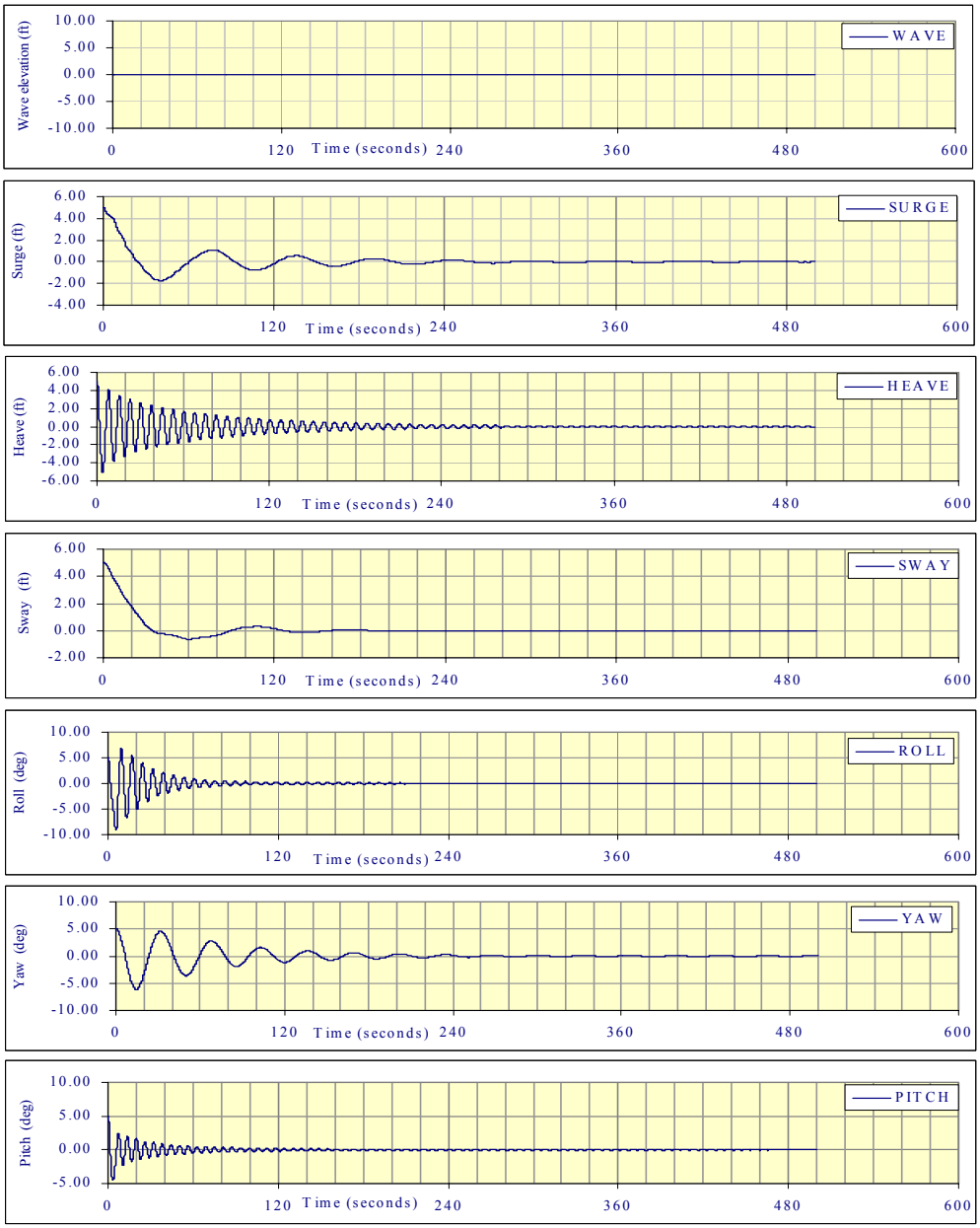


Figure 19. Free decays of MHP Test Bed.

Wave Height. Ship response is highly dependent on wave frequency and is less sensitive to wave height in mild to moderate seaways. At a constant frequency, its motion may be scaled in proportion to the wave height. However, this correlation should not be extended to high sea states, particularly in the case of a flat platform with low freeboard. Motion responses of the present Test Bed to high sea states are expected to be highly nonlinear. Primary sources of nonlinearities include fluid viscosity and large hull geometry variation. The former has been illustrated in the previous section. With a constant viscous damping coefficient of 400 $lb \bullet sec^2/ft^3$, the simulation code was further tested for its sensitivity to regular waves with the wave height over a wide range from 1 foot to 14 feet. All cases were done at the same wave period of 7.5 seconds. Figure 20 summarizes the resulting motion RAO that clearly illustrates the anticipated

strong nonlinearity in the roll responses. Wave height influences roll responses much more than it does the heave motion as anticipated. It is obvious that this nonlinearity does not directly correlate to the wave height alone. The sharp reduction of RAO at the low wave heights implies the quadratic growth of the viscous damping as the platform rolls faster in higher waves. The rebound of roll RAO for wave exceeding 8 feet, on the other hand, reflects the increasing level of deck immersion. This unique feature is detrimental to the dynamic stability of a low freeboard platform. Simulation codes that are not tracking the instant wetted hull shape closely are unlikely to capture this effect.

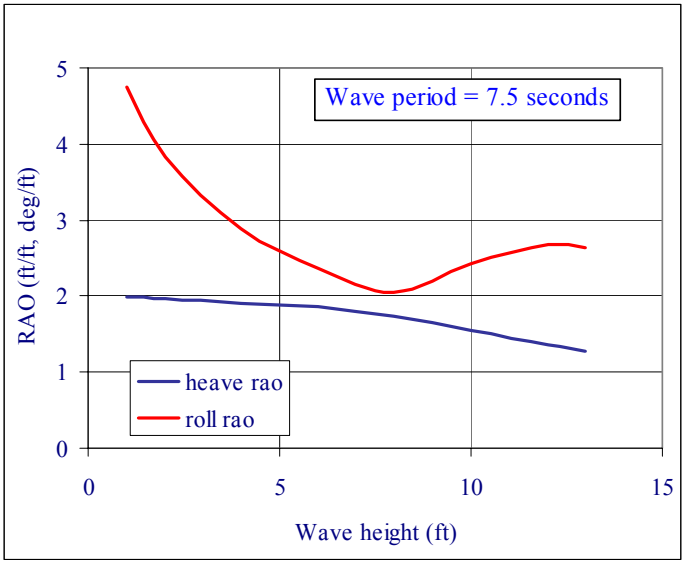


Figure 20. Influence of wave heights on the motion responses.

Center of Gravity. The elevation of center of gravity directly impacts the restoring capacity of a vessel. This series of tests were conducted in beam seas with random waves of 6-foot significant wave height and peak period of 8 seconds. The elevation of the center of gravity was set to 12.35, 14.35, 15.35, and 16.35 feet above keel, respectively. Figure 21 summarizes the effect of the center of gravity. Note that the maximum right arm of the Test Bed as designed is less than 2 feet at the heel angle of 15 degrees as shown in Figure 12. This test series confirms that a high center of gravity will seriously erode the restoring capacity of the Test Bed. The platform of higher center of gravity tends to capsize in lower seaways. As the center of gravity is raised to 16.35 feet above keel (or 2 feet above the designed elevation), the Test Bed rapidly capsizes in 6-foot waves. Exact location of the center of gravity of the Test Bed must be properly verified before departure.


Figure 21. Sensitivity of the elevation of center of gravity to ship stability.

Initial Trim. Stability of a vessel is often assessed in its design draft and attitude. However, it is likely that cargo loads may introduce additional trim to the vessel. For a vessel of limited freeboard, this additional trim may substantially change the submerged hull geometry and thus reduce its stability significantly below the design capacity. Capsizing of small trawlers was repetitively reported in relatively low seas on a good day of abundant catch that lowered its aft deck near water level. The Test Bed is to be ballasted to an average draft of 13.5 feet with a small trim of 0.6 degree by the stern for better towing efficiency. That will leave and average freeboard 6.7 feet to the service deck. Figure 7(b) indicates that the Test Bed in the open configuration will lose more than 50 percent of its stability reservation at a trim angle of 6 degrees. Therefore, a test series was conducted to further explore the sensitivity of the initial trim angle to the dynamic performance of this platform. The open box case at three different initial angles of 0, 2, and 5 degrees from the even keel attitude as shown in Figure 22(a) was simulated in random seaways to identify the lowest seaway that is capable of overturning the Test Bed at

the respective trim angles. Note that, at the initial trim of 5 degrees, the service deck just dips under the water surface at the stern. It is well known that the dynamic performance of a platform is highly frequency dependant. However, for the sake of fair comparison, all simulations of this series were done in random seas with the peak energy period at 9.7 seconds. A seaway of significant wave height 1 foot less than this severity will be assigned as the threshold seaway. The threshold seaways so determined for cases with various initial trims are then summarized in Figure 22(b). It is clear that the influence of initial trim on the ultimate stability of this platform accelerates as the initial trim angle increases. At an initial trim of 5 degrees, the Test Bed tends to capsize in a seaway 4 feet lower than would it in the even keel. However, this Test Bed is to be towed at a small initial trim of 0.6 degree. The stability reduction is expected to be rather limited according to the simulation results. Figure 23 summarizes the seaway performance of the Test Bed at each of the three selected initial trim angles.

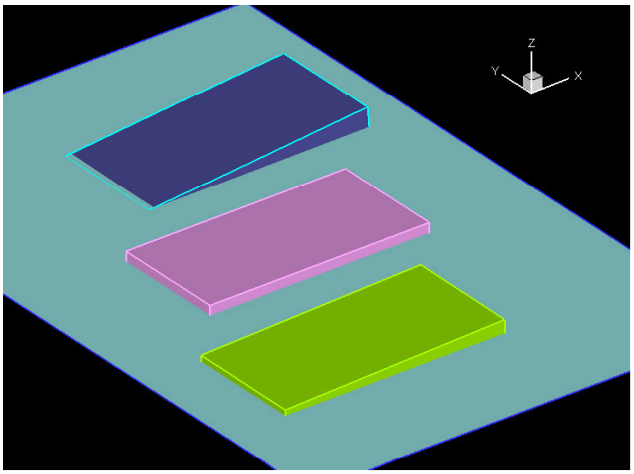


Figure 23(a). Initial trim in degrees, 0 (pink), 2 (green), and 5 (blue).

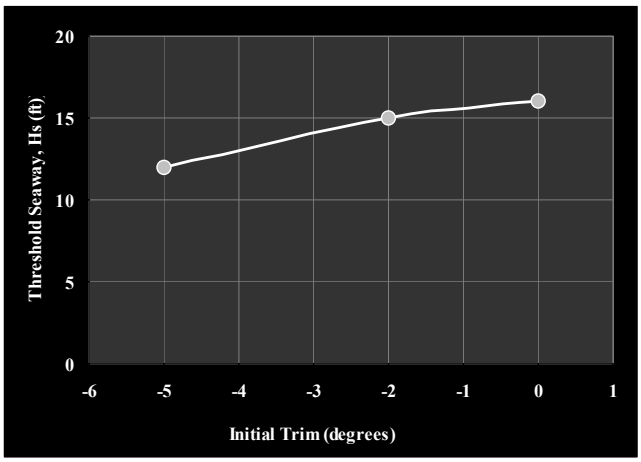


Figure 23(b). Threshold seaway reduction due to initial trim angle.

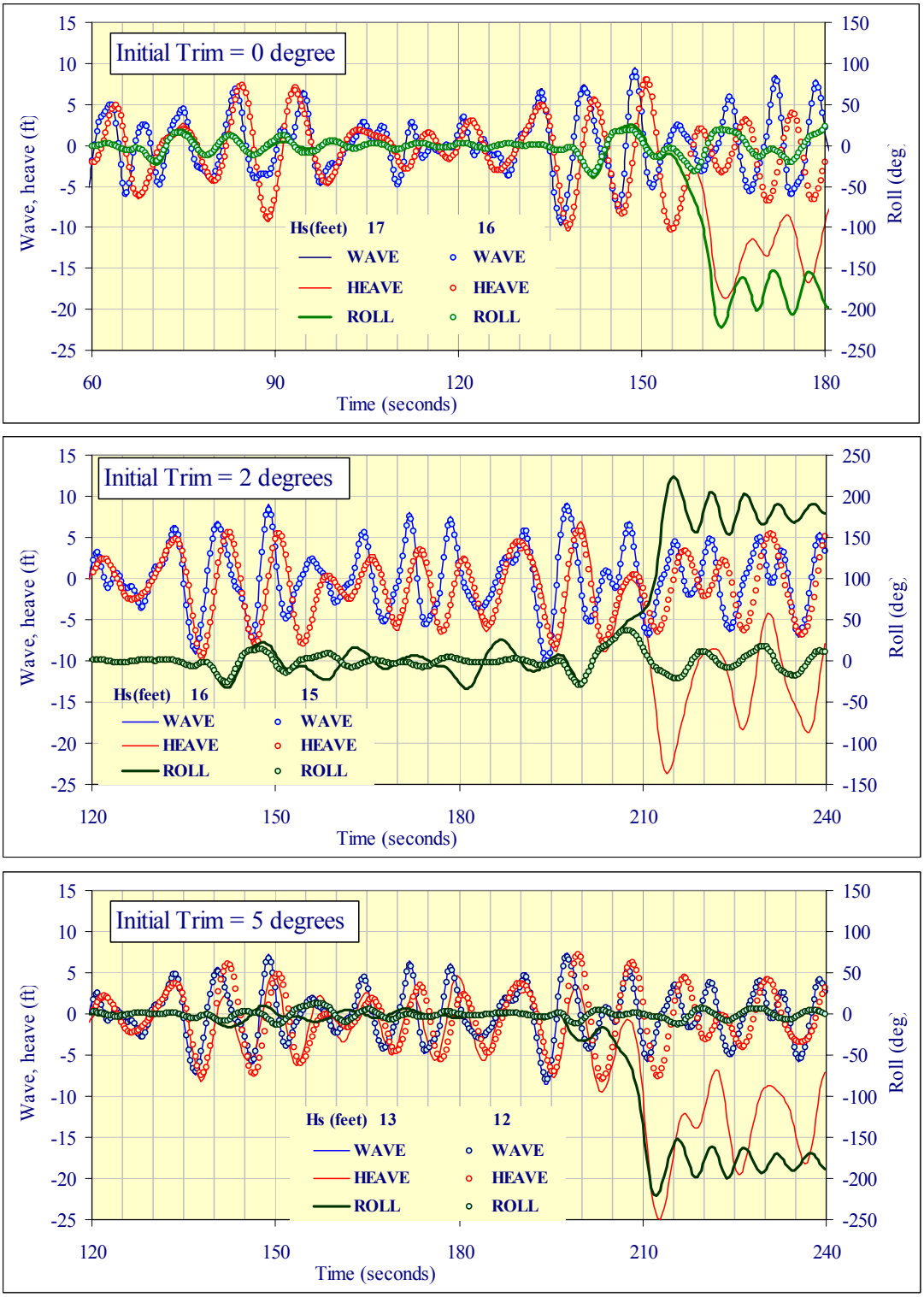


Figure 23. Motion histories of the open box with various initial trims near capsizing.

**Numerical Model Setup for Seaway Performance Analysis**

Layouts of the numerical model are selected based on the findings of the preliminary simulation. The model platform is lightly moored, as illustrated in Figure 14, to prevent the Test Bed from drifting out of the intended course and heading. Four horizontal lines 5,000 feet long are attached to the ends of the Test Bed along its centerline at the elevation of its center of gravity. Soft lines of 1,000 pounds per foot are used to allow a reasonable sway comparable to the anticipated fishtailing of the Test Bed under tow and minimize the possibility of tripping the Test Bed. Damping cylinders of negligible diameter are attached to the four horizontal edges around the flat keel. The equivalent damping forces are controlled by the damping coefficient of $C_d$. A value of 400 is recommended. Other parameters are summarized in Table 6. The coordinate references for platform motion and wave headings are also defined in Figure 12.

Table 6. Parameters Used in the Seaway Performance Simulation

| **Parameters** | **Values** | **Units** |
|---|---|---|
| Displacement | 4.32 | Million pounds |
| Length, Lpp | 100 | feet |
| Beam, B | 50 | feet |
| Deck height, D | 29 (closed box), 17.67 (open box) | feet |
| Draft, d | 13.5 | feet |
| Height of center of gravity | 14.35 (above keel) | feet |
| Gyradii, rxx, ryy, rzz | 14.43 (roll), 28.87 (yaw), 28.87 (pitch) | feet |
| Initial trim and heel | 0, 0 | degrees |
| Mooring well | Excluded | |
| Towing speed | 0 | knots |
| Wind | 0 | knots |

**Seaway Performance**

It has been determined that the Test Bed is most vulnerable to beam seas with their peak energy periods aligned with the nature period of the platform. Consequently, severe beam seas of wave period at 7.5 seconds are chosen to stimulate the platform to the extreme. Both swells and random seas are included. Tables 7 and 8 list the parameters of these model seaways for the two candidate configurations, respectively. Noteworthy findings pertinent to the stability assessment for ocean towing are discussed herein.

At this period, the open box was found to capsize in random seas of significant wave height equal to 12 feet and survive a wave height of 10 feet in beam seas (Figure 24). However, the same platform withstands quartering seas exceeding 12 feet high. It also survives a low Sea State 6 (Hs=13 feet and To=9.7 seconds), if only realistic wind induced seaways are considered. This implies the open box is very likely to survive low Sea State 5 during open sea transit. The closed box is clearly more stable. It comfortably survives the worst-case theoretical seaway of 20-foot waves and realistic seaways above Sea State 7.

Table 7. Wave Parameters Used in Seaway Performance Analysis of Open Test Bed

| Run ID | Wave type | Wave height | Wave period | Wave heading | Notes |
|---|---|---|---|---|---|
| | | feet | seconds | degrees | |
| Boxo_90_r05_h10 | Irregular | 14 | 7.5 | 90 | Capsized |
| Boxo_90_r06_h10 | Irregular | 10 | 7.5 | 90 | |
| Boxo_90_r16_h10 | Irregular | 10 | 7.5 | 90 | |
| Boxo_00_r17a_h12 | Irregular | 12 | 7.5 | 0 | |
| Boxo_45_r17b_h12 | Irregular | 12 | 7.5 | 45 | |
| Boxo_90_r17_h12 | Irregular | 12 | 7.5 | 90 | Capsized |
| Boxo_135_r17c_h12 | Irregular | 12 | 7.5 | 135 | |
| Boxo_180_r17d_h12 | Irregular | 12 | 7.5 | 180 | |
| Boxo_90_s03 | Irregular | 4.6 | 6.5 | 90 | Sea state 3 |
| Boxo_90_s04 | Irregular | 8 | 8.1 | 90 | Sea state 4 |
| Boxo_90_s05 | Irregular | 12 | 9.7 | 90 | Sea state 5 |
| Boxo_90_s06H | Irregular | 18 | 11.3 | 90 | Sea state 6, Capsized |
| Boxo_90_s06M | Irregular | 15 | 9.7 | 90 | Mid Sea state 6, Capsized |
| Boxo_90_s06L | Irregular | 13 | 9.7 | 90 | Low Sea state 6 |

Table 8. Wave Parameters Used in Seaway Performance Analysis of Closed Test Bed

| Run ID | Wave type | Sig. height | Peak period | Heading | Notes |
|---|---|---|---|---|---|
| | | Feet | Seconds | Degrees | |
| Boxc_90_r17a | Irregular | 12 | 7.5 | 90 | |
| Boxc_90_r17b | Irregular | 15 | 7.5 | 90 | |
| Boxc_90_r17c | Irregular | 20 | 7.5 | 90 | |
| Boxc_90_r20a | Irregular | 15 | 10 | 0 | |
| Boxc_90_r20b | Irregular | 15 | 10 | 45 | |
| Boxc_90_r20c | Irregular | 15 | 10 | 90 | |
| Boxc_90_r20d | Irregular | 15 | 10 | 135 | |
| Boxc_90_r20e | Irregular | 15 | 10 | 180 | |
| Boxc_90_r30a | Irregular | 15 | 10 | 90 | 60% wave damping |
| Boxc_90_r30b | Irregular | 15 | 7.5 | 90 | 60% wave damping |
| Boxc_90_r30c | Irregular | 20 | 7.5 | 90 | 60% wave damping |
| Boxc_90_r30d | Irregular | 20 | 10 | 90 | 60% wave damping |
| Boxc_90_s03 | Irregular | 4.6 | 6.5 | 90 | Sea State 3 |
| Boxc_90_s04 | Irregular | 8 | 8.1 | 90 | Sea State 4 |
| Boxc_90_s05 | Irregular | 12 | 9.7 | 90 | Sea State 5 |
| Boxc_90_s06 | Irregular | 18 | 11.3 | 90 | Sea State 6 |
| Boxc_90_s07 | Irregular | 40 | 15.4 | 90 | Sea State 7 |

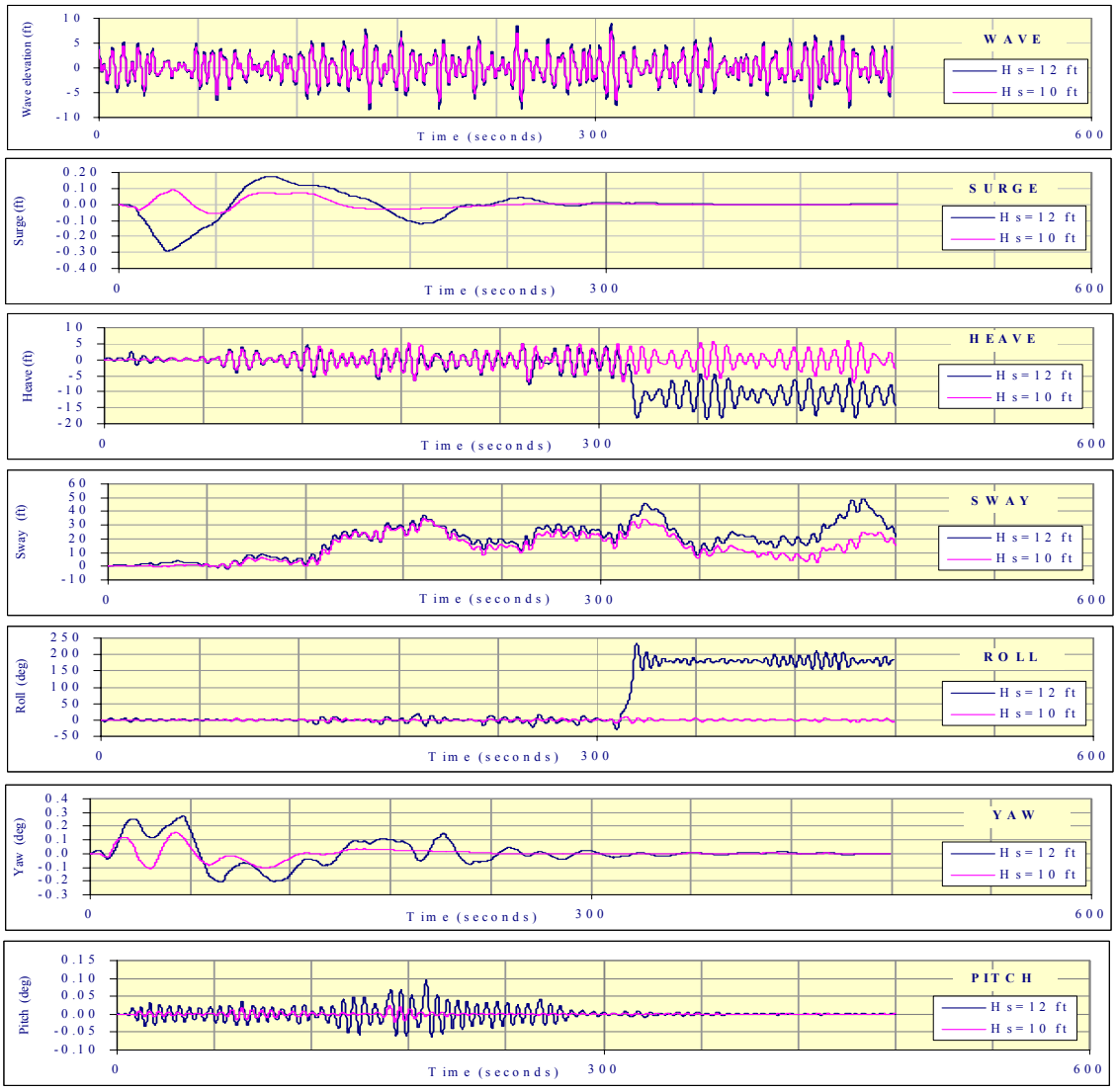


Figure 24. Performance of the open box in beam seas of Hs=10 ft (red) and Hs=12 ft (blue), with Tp=7.5 seconds.

## Capsizing Process

The open box capsizes in a theoretical seaway of 12-foot waves with peak period at 7.5 seconds (Case Boxo_90_r17_h12), and in the mid Sea State 6 with wave a height of 15-foot and peak period at 9.7 seconds (Case Boxo-90_s06M). These cases were reviewed to investigate the capsizing process. Figure 25 displays the wave activity as well as roll and heave responses of these cases near the moment of capsizing. Note that the combination of large heave and wave excursion creates a vulnerable moment of extremely low stability as a result of severe deck immersion signified by large downward relative heaves. The platform heels extensively when a large relative heave occurs amid a high wave group. The roll motion slows down noticeably and its phase angle relative to wave constantly changes in time. This allows adverse wave groups to align with the platform in its critical attitude of the least stability and knock the platform over. Similar behavior was also observed with a deck barge in the wave basin (Figure 26) reported by

Huang et al. (Reference 12). Figure 25a presents a sequence of images captured at the moment of barge capsizing. The freeboard was 2 feet in this case and the capsizing took place in Sea State 4. A large quantity of green water constantly swept across the deck throughout this test run. The barge drifted extensively and often hung in a large heel angle after being hit by a large wave. Capsizing took place when a steep wave appeared at the moment while the barge hung in a large heel toward waves as shown in the first frame of Figure 26. Timing is critical. The wave variability in random seas offers greater opportunities to see this adverse combination. In fact, this test confirmed that random seas are more likely to capsize the barge than swells.

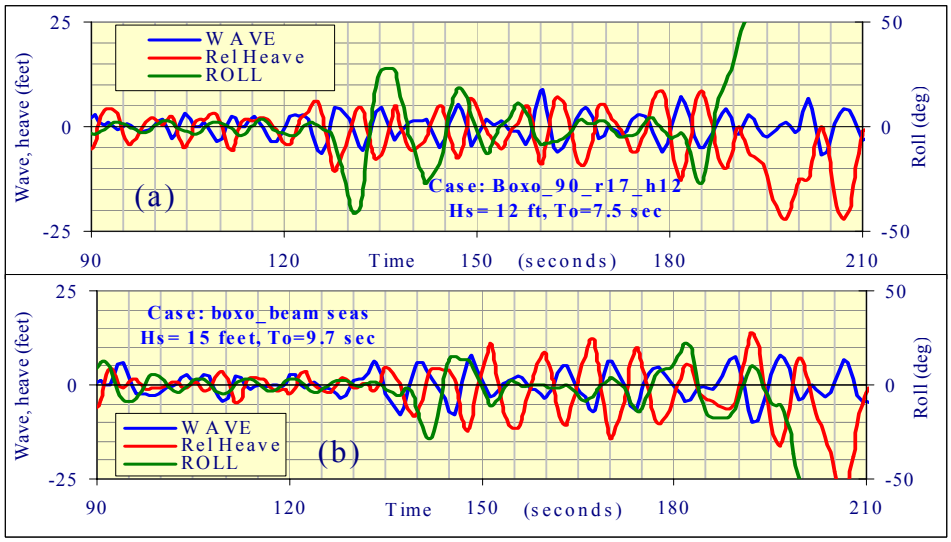


Figure 27. Wave and motion activities before capsizing.

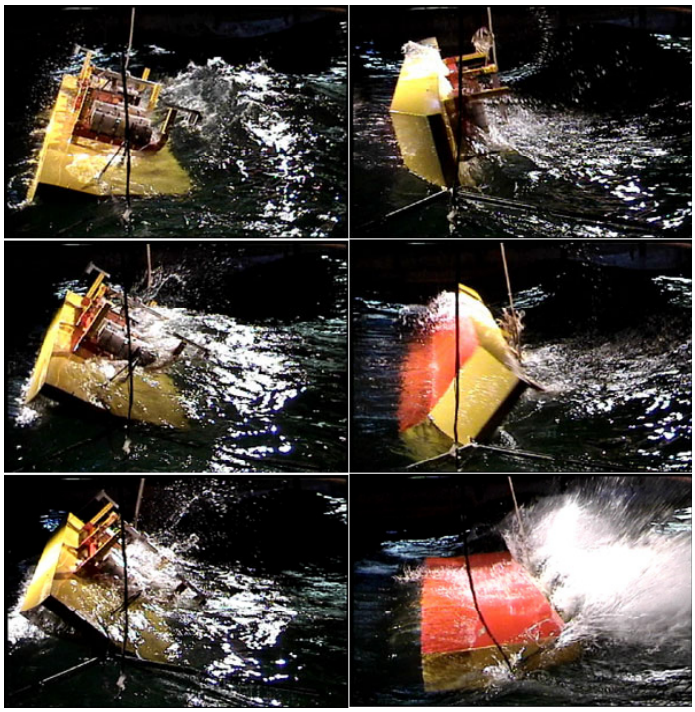

Figure 26. Barge capsizes in random seas (Huang et al, 2001).

The closed box, on the other hand, survives the limiting Sea State (Hs=12 feet and To=7.5 seconds) that capsized the open box. Figure 27 (a) and (b) compares motion responses of these two boxes in their time histories (Figure 7a) and power spectral density functions (Figure 7b). Motion spectra of the open box were deduced from motion histories prior to capsizing. It is clear that these two boxes react quite differently. The open box rolls tremendously stronger than the closed box with a distinct low frequency drift that eventually capsizes the box. Both boxes heave in the window of dominating wave energy. But, the closed box reacts twice as much as the open box.

The roll energy of the open box penetrated so deeply in the frequency band of little wave energy that is hard to attribute to the wave nonlinearities alone. This more likely reflects the dramatic geometry change in its wetted hull as the service deck falters near the water surface. The constantly changing restoring stiffness causes the open box to change pace in time. Once the service deck immerses, the platform loses its resistance to heeling moment. The static heeling moment also disappears in the mean time. Thus, the platform rolls easily at a slow pace subject to dynamic heeling moment. It also loses the heave stiffness under this circumstance, but retains a constant, positive heaving force equal to the excessive buoyancy over its displacement. This excessive heaving force prevents the platform from drifting extensively. Therefore, the open box heaves relatively milder than the closed box once the service deck immerses. This low frequency roll drift does not appear with the closed box because it rarely fully immerses under the water surface, even in Sea State 7. This gives the closed box tremendously more stability than the open box. The same can also be observed from the motion histories of these two boxes presented in Figures 28 and 29. In Figures 28 and 29, wave and motion activities were split at the period of 20 seconds into high frequency and low frequency components. Note that the low frequency components (green lines) refer to the right scales. Overall, the high frequency components indicate that the closed box heaves stronger, but rolls much less than the open box. Nevertheless, the open box drifts more extensively than the closed box in both heave and roll modes. This leads to a detrimental difference to the ultimate stability of the platform. The heave drift of the open box is clearly biased to the down side. The service deck actually stays submerged longer than it does above the water surface. This allows the open box to roll dramatically more than the closed box: twice in the high frequency component and ten times in the low frequency drift. A good example can be seen in Figure 29 around the 260-second mark. A large down side heave deeply submerges the service deck below the water surface and allows the platform to heel more than 20 degrees without exposing the service deck. In fact, the open box capsizes at the next large wave cycle.

To further confirm the thought, motion responses of the open box to a 10-foot seaway is also presented in Figure 30. The platform comfortably survives this seaway. Both heave and roll motion spectra are very similar to those of the closed box case in a 12-foot seaway. The high frequency heave in a 10-foot wave is only slightly less than that in a 12-foot wave, however, the low frequency component is only 30 percent. The capsizing is clearly connected to the significant low frequency drifting attributed to severe deck immersion. The additional freeboard of the closed box apparently makes all the difference.

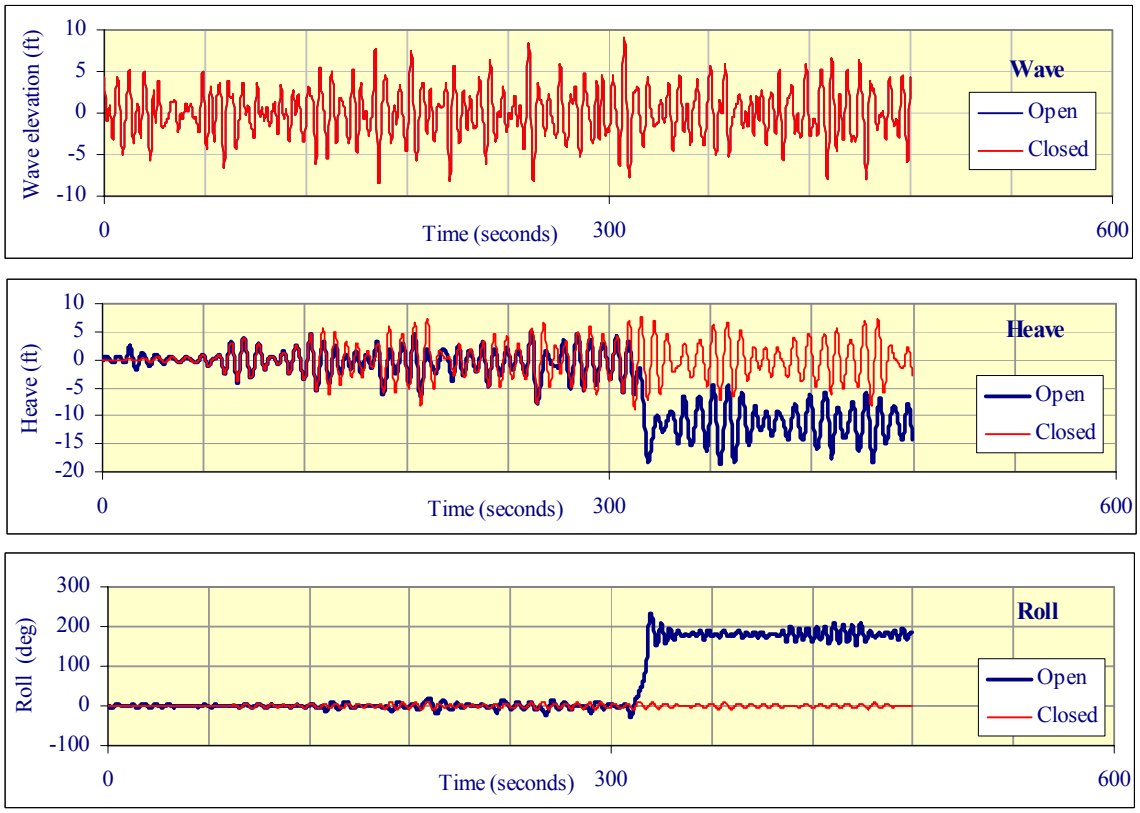


(a) Time histories

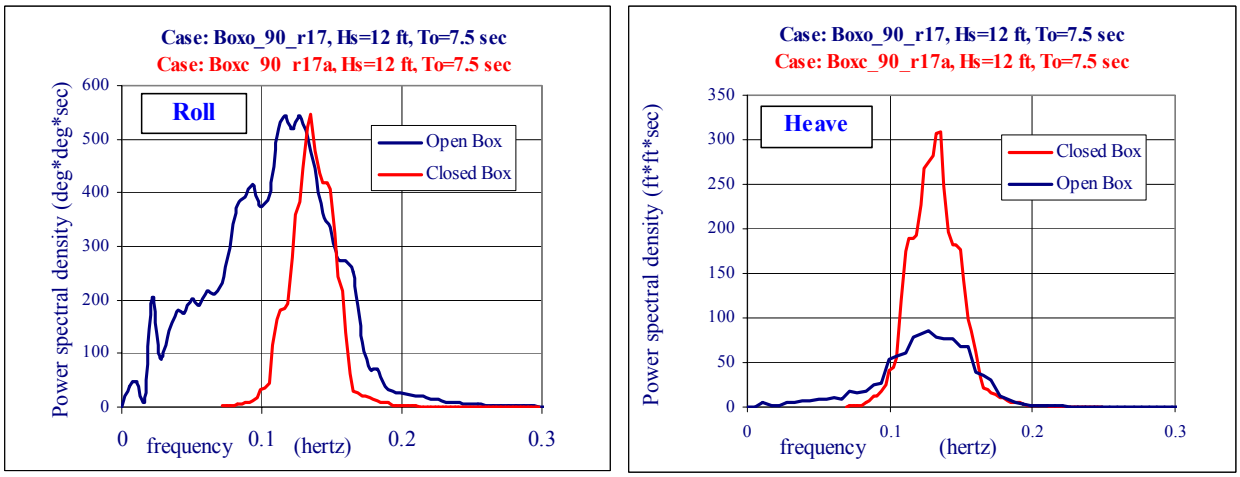


(b) Power spectral density

Figure 27. Effects of barricades above service deck.

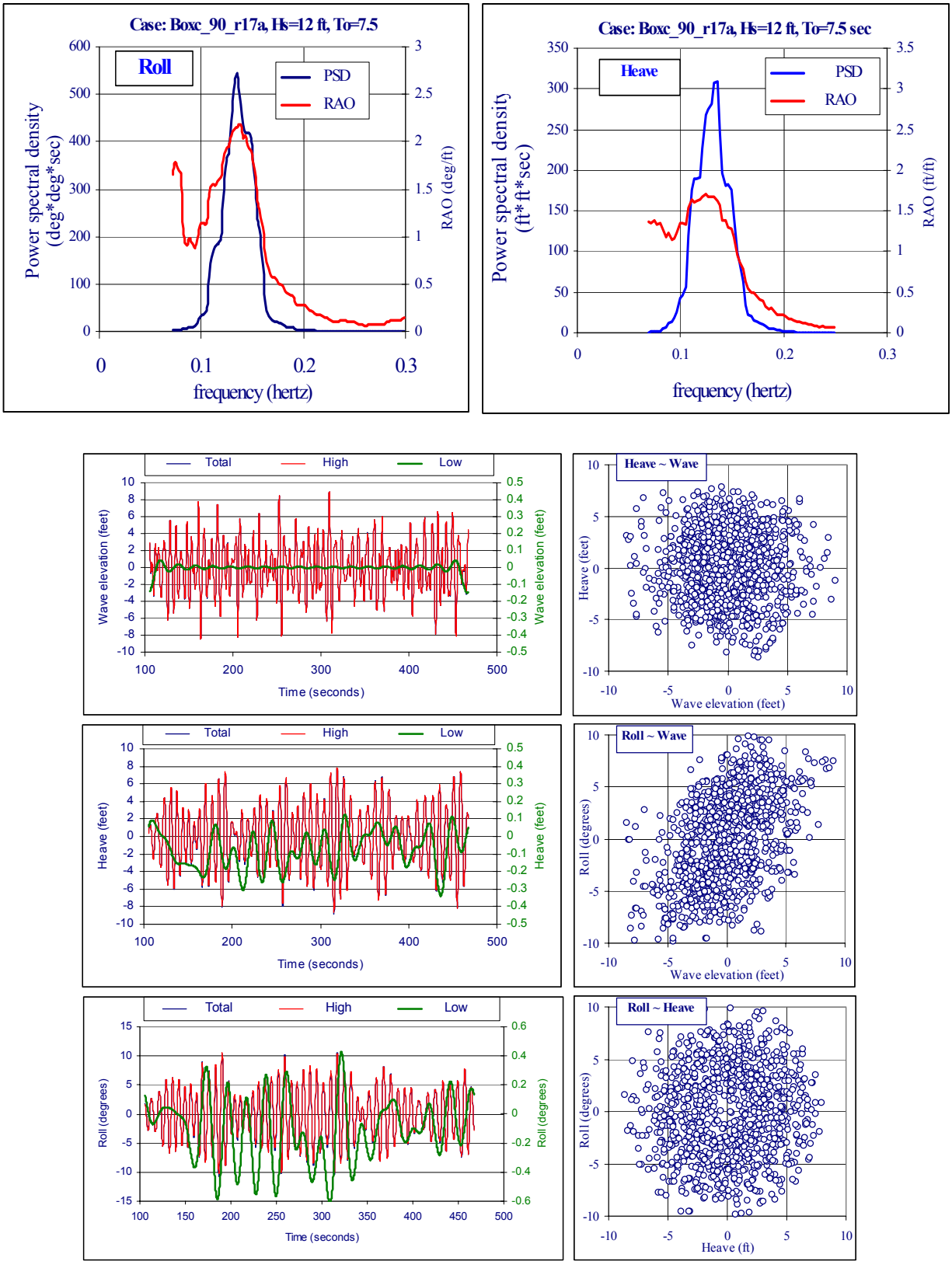


Figure 28. Case Closed Box, Beam seas, Hs=12, To=7.5.

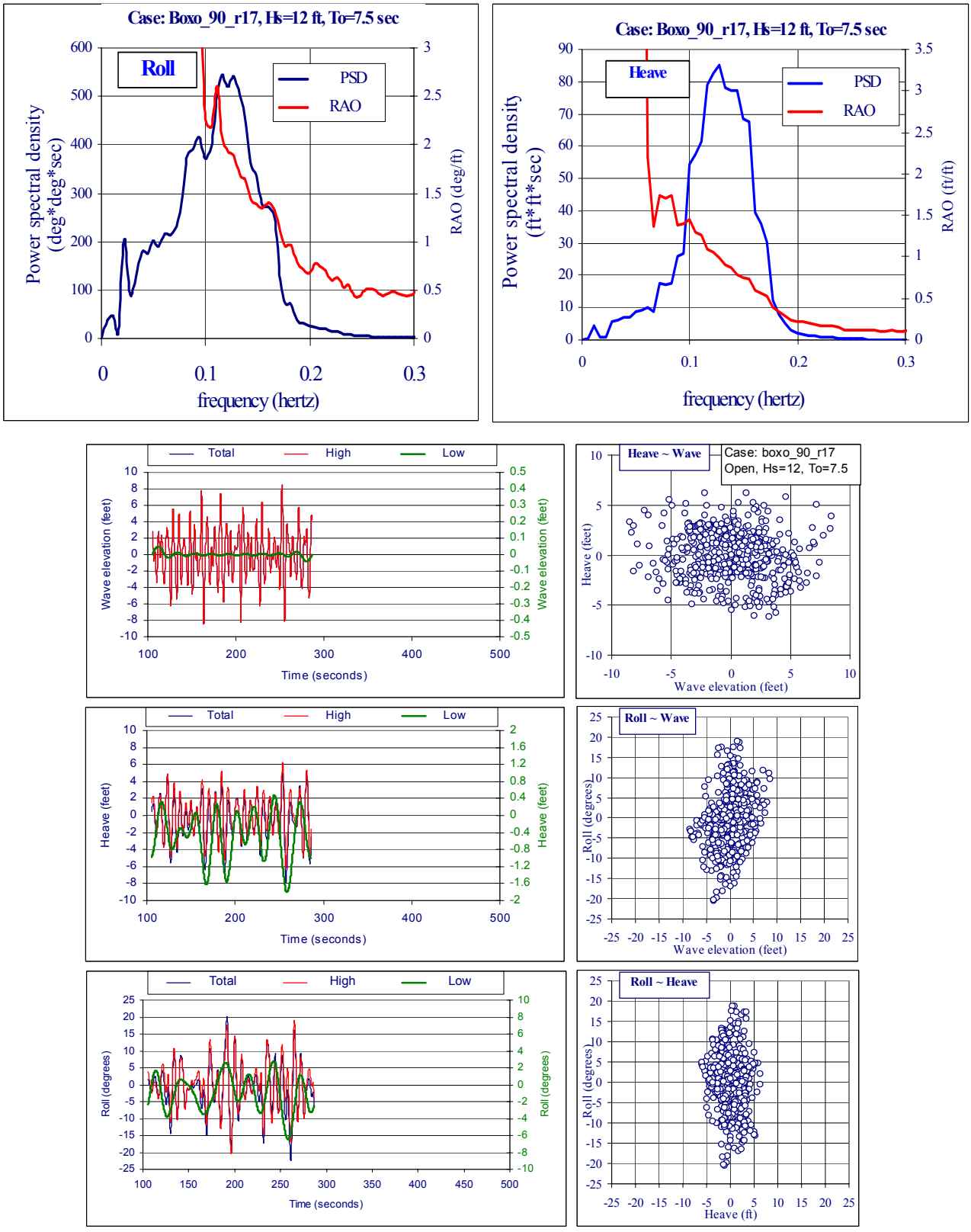


Figure 29. Case Open Box, Beam seas, Hs=12, To=7.5 (512 data before capsizing).

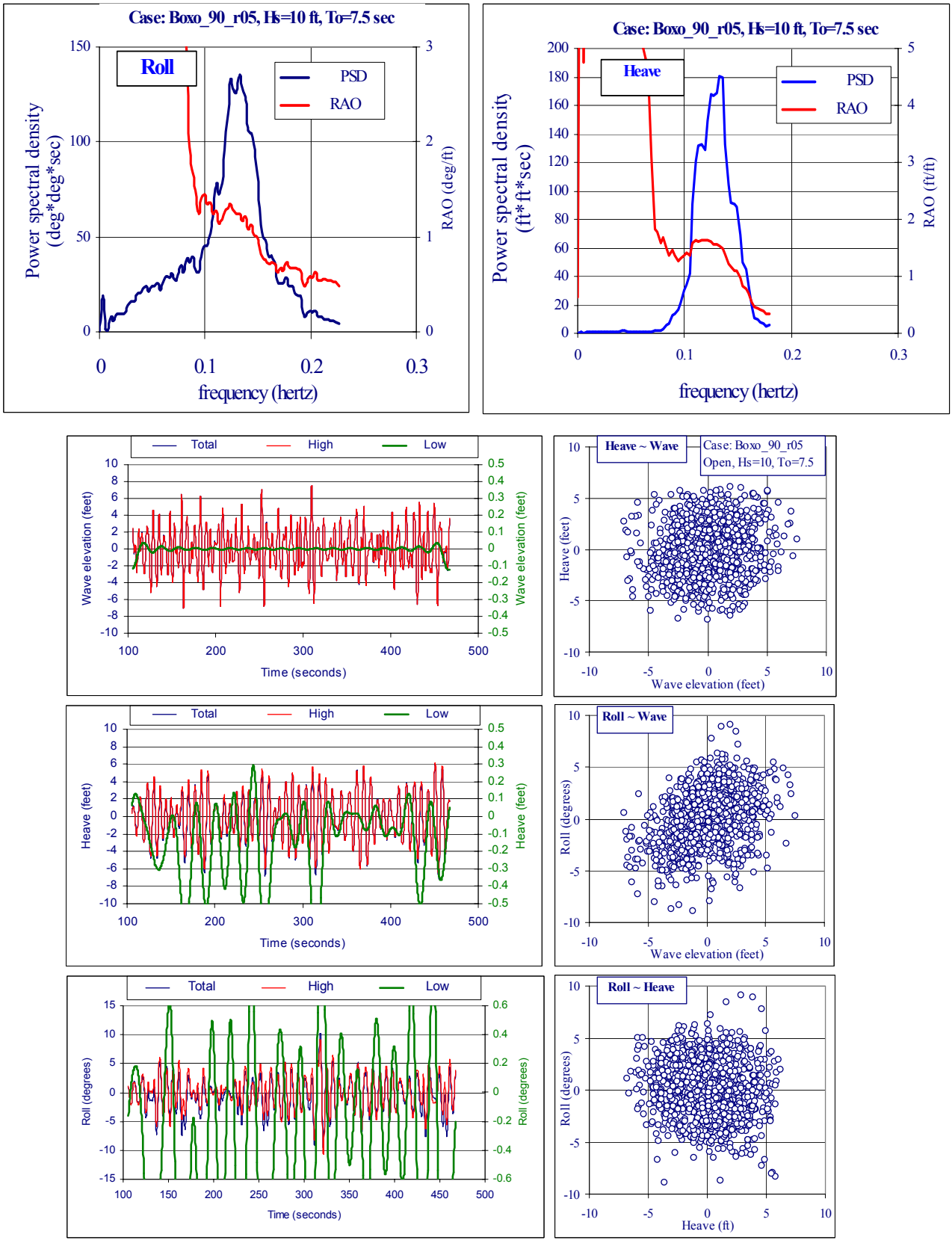


Figure 30. Case Boxo_90_r05, Open Box, Beam seas, Hs=10, To=7.5.

**Threshold Seaway**

Capsizing is a rare incident and seaways linked to the casualties are seldom well documented. The possibility for this platform to run into uncharacteristic seaways cannot be completely ruled out. Therefore, this assessment considers both theoretical seaways that are likely to excite the platform to the limits and the standard model seaways that are more likely to see during this ocean tow. Bretschneider's two parameter spectra retain the flexibility of representing unusual seaways.

Theoretical seaways. This proposed ocean towing sets a survival criterion at Sea State 6. The significant wave height and period at the peak energy associated to a mid Sea State 6 seaway as recommended by the sea state chart in Appendix A are 15 feet and 10 seconds, respectively. The closed box will be further appraised against this seaway as well as a theoretical seaway of the same intensity but with a shorter peak energy period of 7.5 seconds. Its seaway performances are presented in Figures 31 and 32. Results indicate that the platform comfortably survives both seaways, showing no sign of capsizing. All motion responses are higher but of the same nature as those of the corresponding seaways of 12 feet high. No obvious drift was observed in either the heave or roll. The scattering diagrams indicate motions in a 10-second seaway are somewhat better correlated to wave actions than those in a 7.5-second seaway. This implies that the Test Bed follows the longer waves closer and thus experiences smaller relative motion. Figure 33 indicates that the operational deck starts to occasionally immerse under the water surface in a 15-foot seaway with 7.5 second peak period. The top charts of Figure 34 clearly illustrate the motion reduction as the peak energy period increases from 7.5 to 10 seconds. The associated RAOs deduced from two seaways (bottom charts) are identical, because this function depends on hull characteristics alone. Also shown in these charts are the corresponding wave spectra. It can be seen that the seaway with a peak period of 7.5 seconds is better aligned with both heave and roll RAOs. Higher motion response is thus a direct consequence. The thin lines in these charts are wave spectra.

The closed box was then tested against a higher seaway of 20 feet. Results of the seaway performance are presented in Figure 35. The Test Bed still shows no sign of capsizing. Nevertheless, it heaves as much as 15 feet up and down at an average speed of 10 ft/sec. The relative heave chart in Figure 36 indicates that more than one half of the keel is being tossed out of the water. This seriously violates the theoretical premises underlying the MULTISIM code. Simulation results in higher seaways are less meaningful.

However, a unique issue was observed from the results to date that the maximum roll amplitude does not increase much as the wave height increases from 12 feet to 20 feet. A series of test runs was thus conducted to verify this trend. In this series, the peak energy period of model seaway is set to a constant value of 7.5 seconds with the significant wave height varying from 2 through 20 seconds. Figure 37 portrays the associated wave spectra. The resulting motion spectra and RAOs are presented in Figure 38. It is noted from the bottom charts of Figure 38 that the platform heaves closely in proportion to wave actions with only slight reductions in the RAO throughout the entire range of wave heights. The roll RAO, on the other hand, drastically reduces as the wave height increases. This result may be attributed to the significance of viscous damping to roll motion responses. As a rule of thumb, viscous damping increases in proportion to the relative velocity square. A faster rolling platform tends to draw higher drag. At a certain point, this drag essentially offsets the increase in heeling moment induced by higher sea states. As a

result, this platform rolls within the same range as the wave height increases from 15 to 20 feet. It is also noted that the operation deck starts to dip under water from time to time in seaways above 15 feet. However, the influence of roll stiffness reduction due to deck immersion does not set in like the case of the open box. The reason is that the closed box, when fully submerged, possesses a small positive stability with its center of buoyancy situated above the center of gravity. The roll RAO continues to decrease monotonously.

A similar test series was conducted to explore the influence of wave period on motion responses. In this case, the significant wave height is set to 15 feet and remains constant throughout the series. The peak energy period is now changing from 6 to 20 seconds. The associated wave spectra are presented in Figure 39. Note that the peak energy period actually dictates the spectral shape. Spectra of longer peak energy period represent younger seas generated by stronger storms. The total energy remains the same. But the energy content is more concentrated around the peak period. The simulation results are summarized in Figure 40. A seaway with its energy distribution better aligned with the motion RAO excites the platform more effectively. Both heave and roll RAOs are not sensitive to the peak energy period.

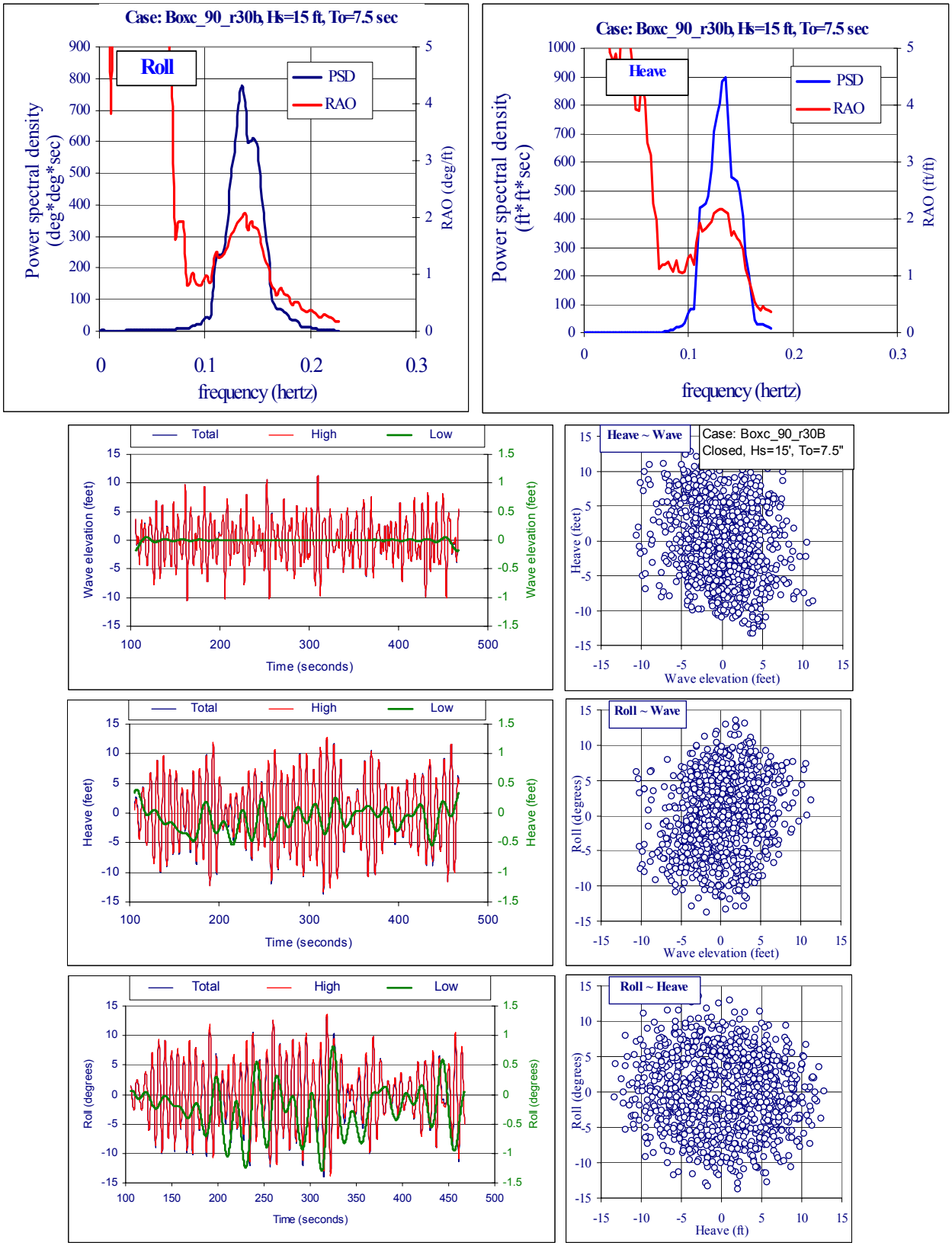


Figure 31. Case Boxc_90_r30b, Beam seas, Hs=15 ft, To=7.5 seconds.

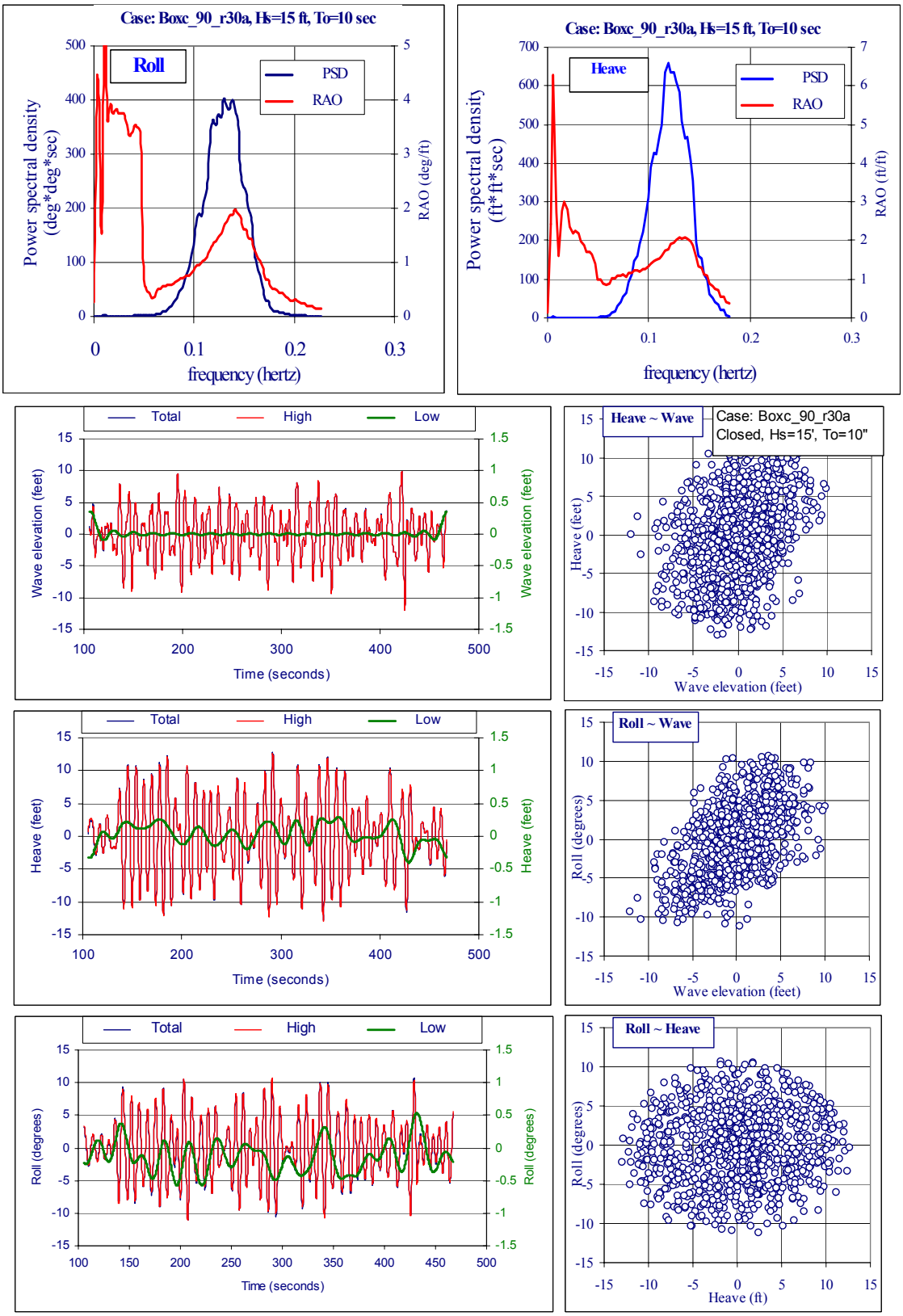


Figure 32. Case Boxc_90_r30a, Beam seas, Hs=15 ft, To=10 seconds.

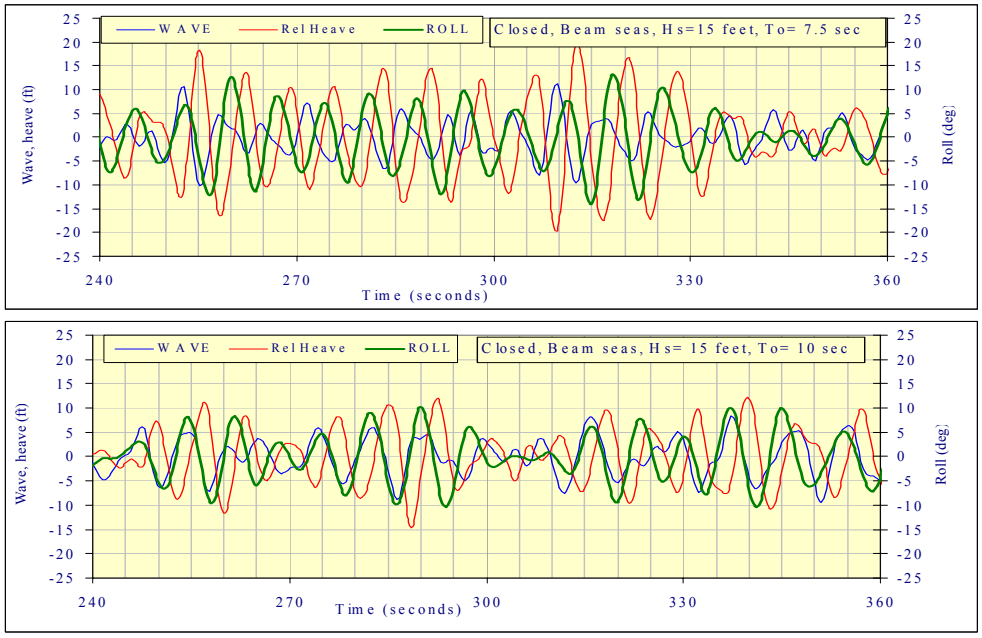


Figure 33. Relative motion of Test Bed to 15 foot waves with To=7.5 and 10 seconds.

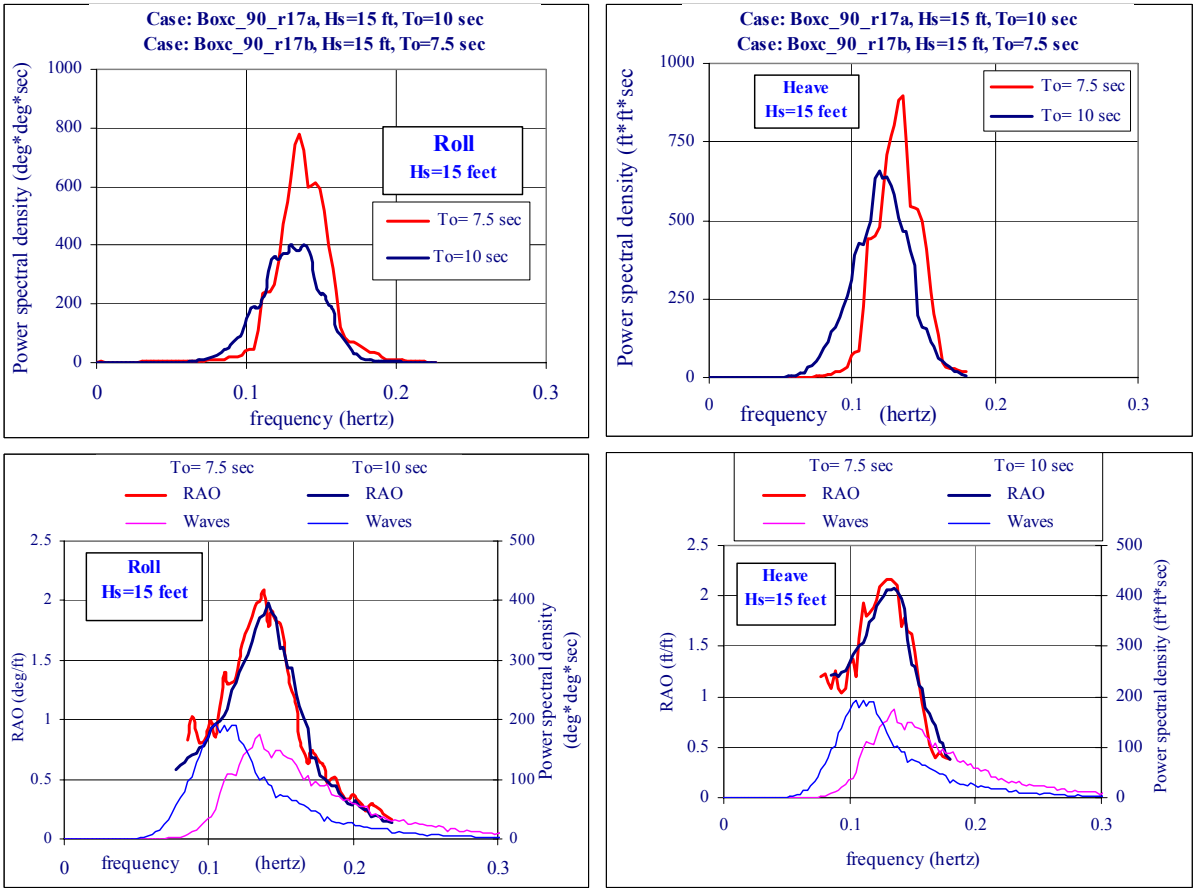


Figure 34. Effect of peak frequency of wave spectrum. +

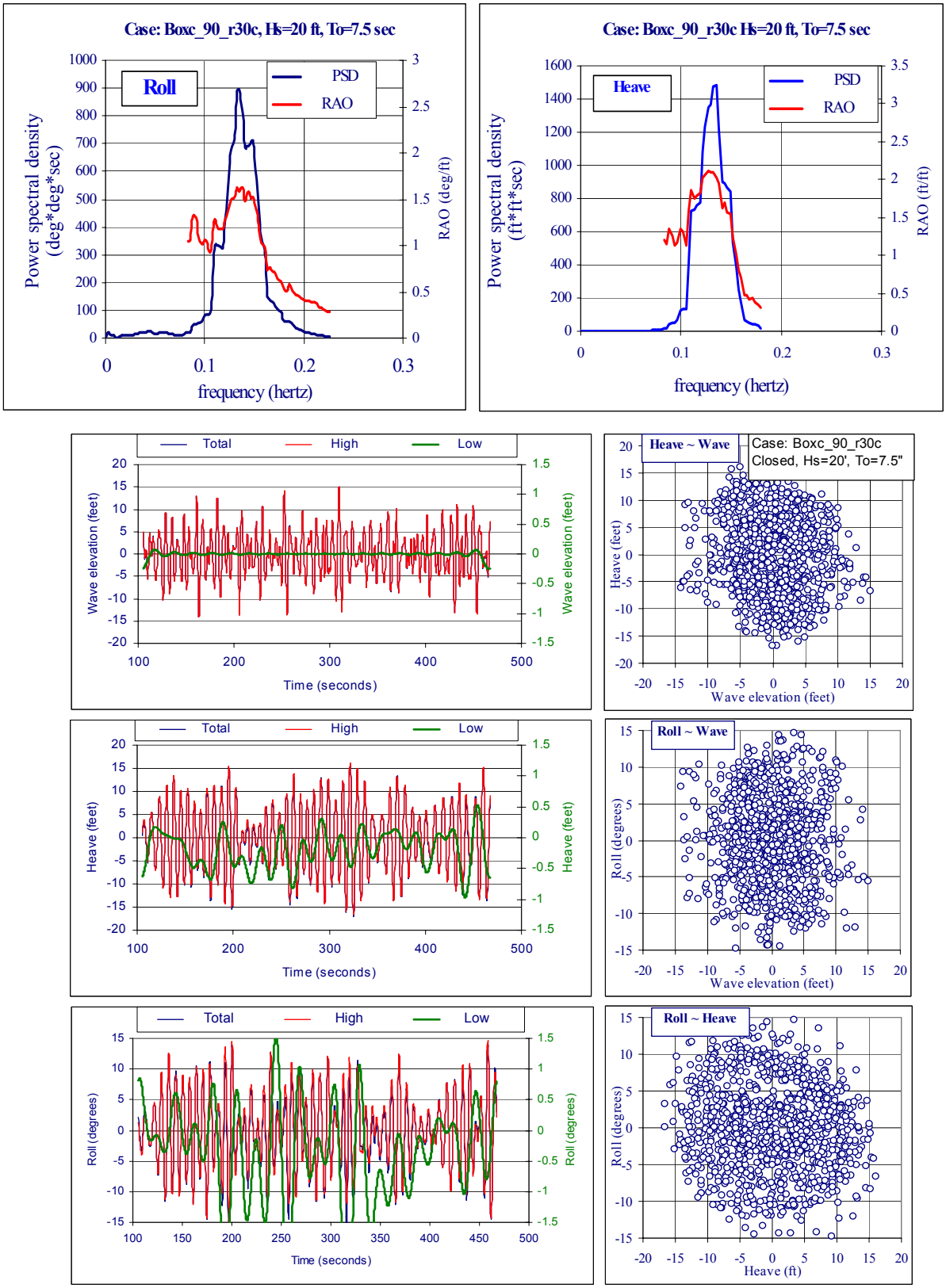


Figure 35. Case Boxc_90_r30c, Beam seas, Hs=20 ft, To=7.5 seconds.

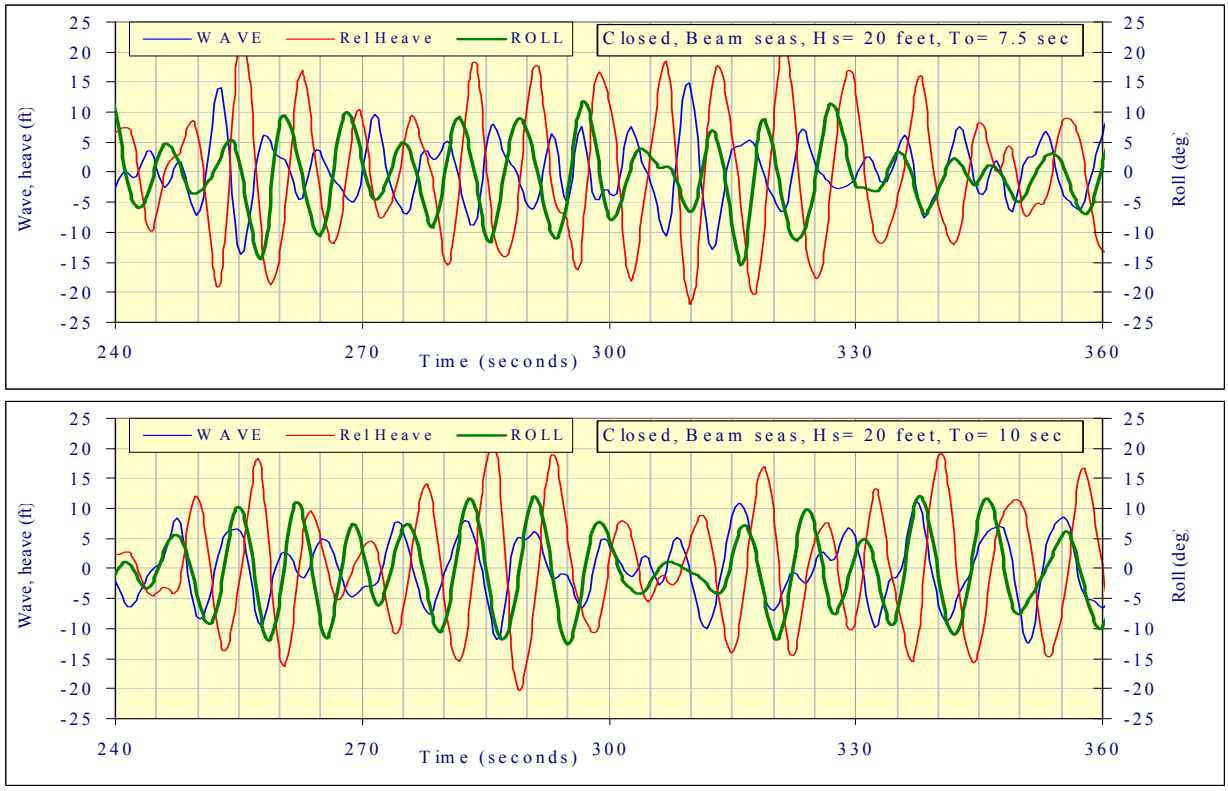


Figure 36. Relative motion of Test Bed to 20-foot waves.

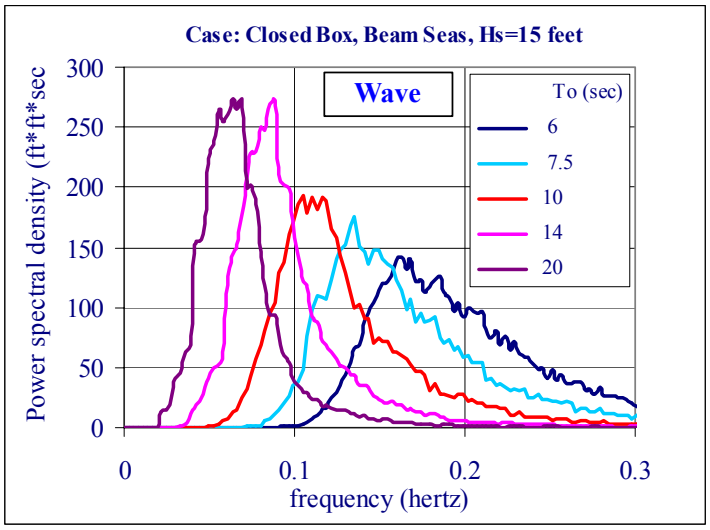


Figure 37. Random seas of peak wave period of 7.5 seconds at various wave heights.

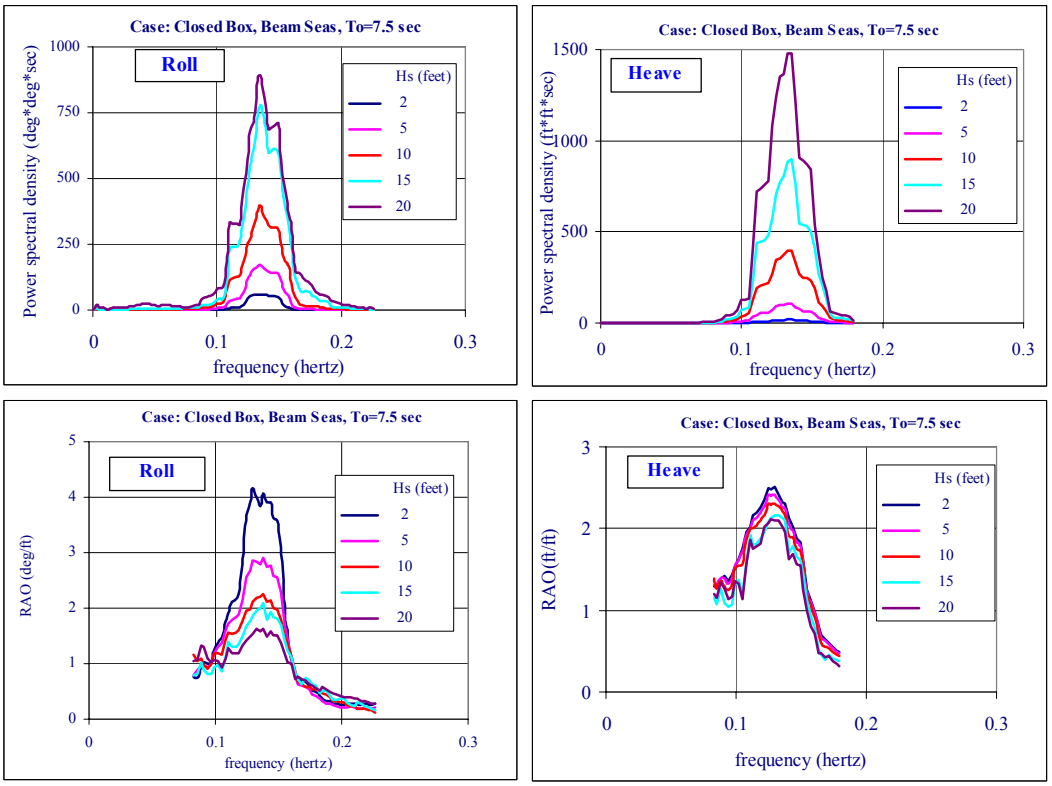


Figure 38. Heave and roll responses to seaways of various wave heights.

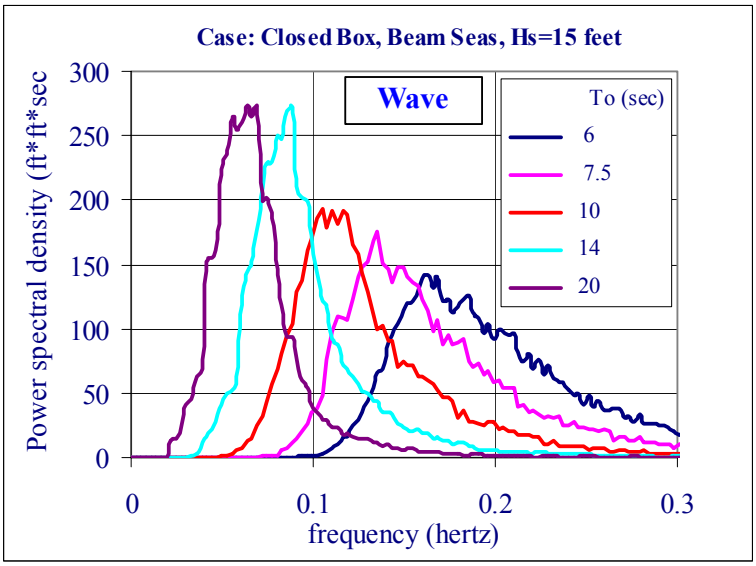


Figure 39. Random seas of significant wave height of 15 feet with various peak energy periods.

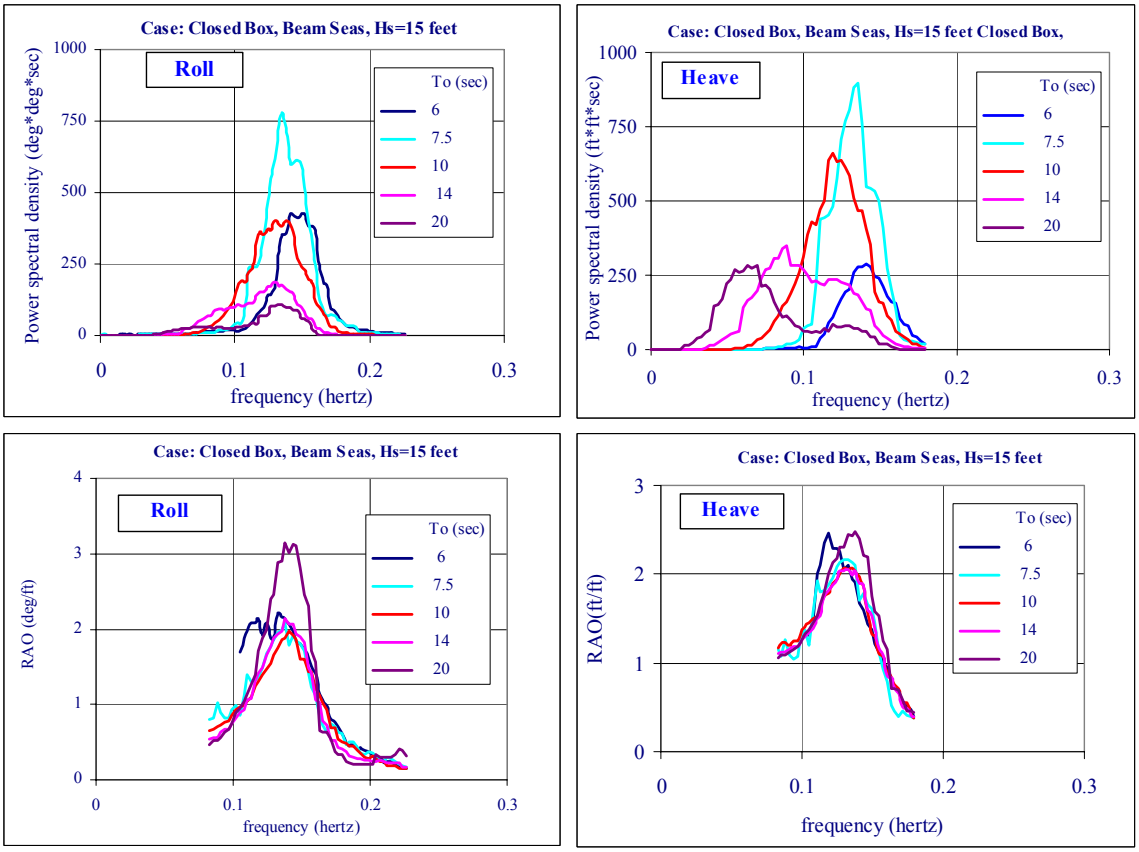


Figure 40. Heave and roll responses to seaways of various wave periods.

Realistic Seaways. The model wave of Hs=15 feet and To=7.5 seconds is much steeper than realistic seaways normally observed in the field. Field data indicate the wave height and wave period of wind generated seas are highly correlated. Wave parameters of real seaways as recommended by a popular Sea State chart compiled by David Taylor Model Basin as shown in Appendix A are listed in Table 9. These parameters represent the upper boundaries of the associated Sea States. Considering the cruise route, season, and the survival criteria set forth for the upcoming ocean tow, the Test Bed may encounter seaways up to Sea State 6. Hence, the seaway performance of this platform in both configurations will be appraised over the range from Sea States 3 to 7. Figure 41 summarizes time histories of the input wave and the motion responses of the closed box in Sea States 4, 5, 6, and 7. Also presented in this figure are the scattered diagrams showing correlations between waves, heave, and roll. The associated wave and motion spectra are presented in Figure 42. Results induced by the theoretical seaway of Hs=15 feet and To=7.5 seconds are presented in dash lines for comparison. Of the four charts in Figure 42, the first three (going counterclockwise from the top left) present the spectral density functions of waves, roll, and heave motions whereas, the last chart shows the statistics of their extreme values as a function of sea state. The symbols Max and Min in this chart indicate the positive and negative extremes of the simulated date set while "1/1000+" and "1/1000-" indicate the most probable extremes in 1,000 cycles. Heave responses in the high frequency band are mostly within the envelope of the baseline case and are significantly more severe in the low frequency band. However, this platform is expected to follow waves longer than 10 seconds closely as indicated by the heave RAOs presented in Figures 39 and 41. As a result, the level of deck immersion will not be much more severe than that of the baseline case. The evidence that roll responses to seaways up to Sea State 6 show no sign of low frequency drift confirms this thought. It takes Sea State 7 to heave the platform to the extent that it immerses the operation deck. This indicates the operation deck immerses quite frequently, and consequently triggers extensive low frequency drifts in roll and heave motions. Sea State 7 is associated to a 40-foot significant wave height, which is far beyond the valid range of MULTISIM code. The result is less meaningful. The extreme roll amplitude in seaway up to Sea State 6 is estimated 15 degrees and the extreme heave about 15 feet. Based on these simulation results, the closed Test Bed is very likely to survive the ocean tow.

Table 9. Sea State Chart

| **Sea State** | **Significant Height (Hs)** | **Period of Maximum Energy (To)** |
|---|---|---|
| | Feet | Seconds |
| 3 | 4.6 | 6.5 |
| 4 | 8.0 | 8.1 |
| 5 | 12.0 | 9.7 |
| 6 | 18.0 | 11.3 |
| 7 | 40 | 15.4 |

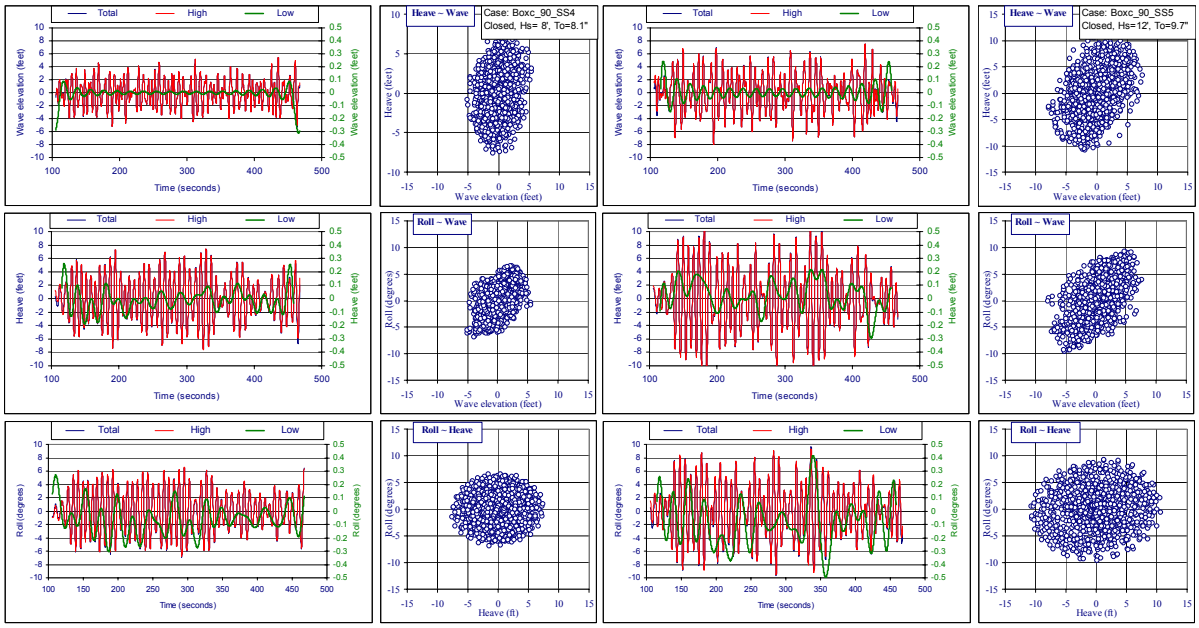


(a) Sea State 4 (b) Sea State 5

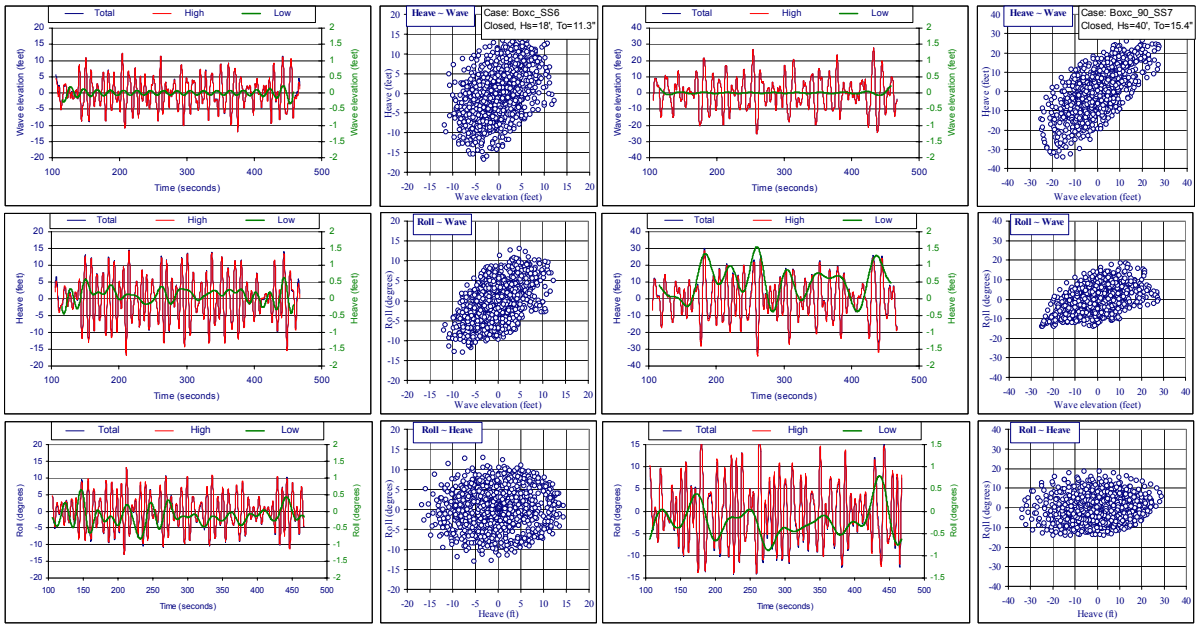


(c) Sea State 6 (d) Sea State 7

Figure 41. Closed box responses to: (a) Sea State 4, (b) Sea State 5, (c) Sea State 6, and (d) Sea State 7.

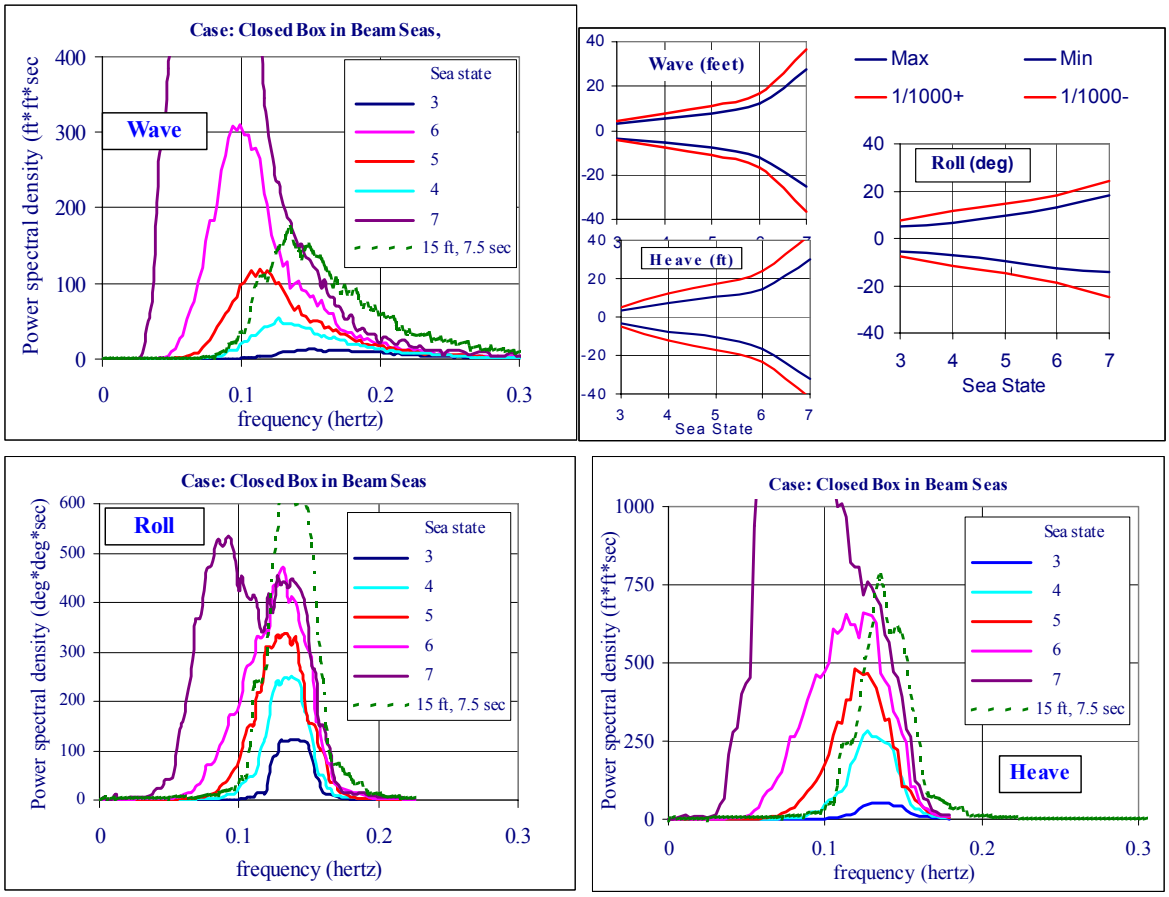


Figure 42. Limit Sea State for the closed Test Bed.

Seaway performance of the open box is further appraised in realistic Sea State 3, 4, and 5 as well as a theoretical seaway of Hs=8 feet, and To=7.5 seconds. Results of motion histories and power spectra are summarized in Figures 43 and 44. The open box surely behaves quite differently than the closed box as shown in Figure 45.The open box rolls identical to the closed box in Sea State 3, slightly higher in Sea State 4, and drastically different in Sea State 5. It heaves less than the closed box in Sea State 5, but still sufficiently vigorous to deeply immerse the entire service deck and create a vulnerable moment allowing the platform to roll extensively as shown in Figure 25(b). The profound low frequency drift in roll motion of the open box in Sea State 5 as illustrated in the lower left chart of Figure 44 is not seen in the low Sea States. The associated motion histories in Figure 43 indicates that the open box sinks more than 10 feet and heels nearly 50 degrees at the extremes in Sea State 5. The platform survives, however, it is believed to be on the verge of capsizing. Since the open box barely survives Sea State 5 and may capsize in a theoretical seaway equivalent to low Sea State 5, its operation should be limited to high Sea State 4.

Figure 46 summarizes the slow roll drifts of the two boxes. The connection of capsizing to the slow drift is clearly illustrated. However, this status of low stability is a consequence of low freeboard rather than low metacentric height as the static criteria assume. Besides, the stability of the platform at an instant depends on the wetted hull shape at the moment, which in

turns is determined by relative phases among heave, roll, and wave activities. This factor is, however, not included in the traditional dynamic criteria.

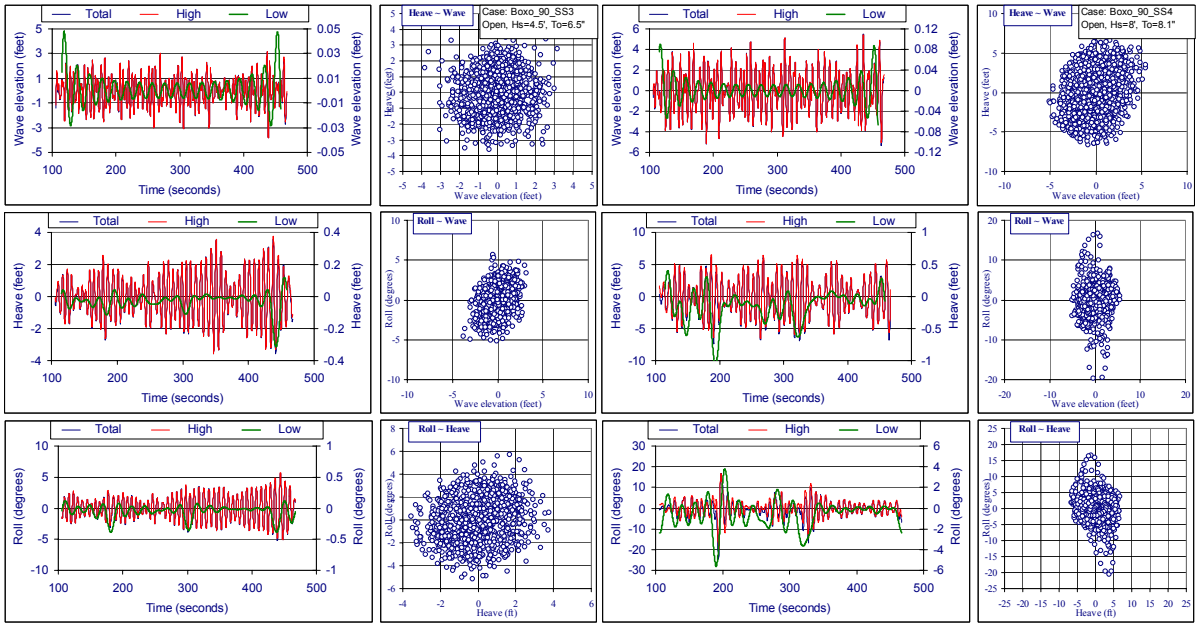


(a) Sea State 3 (b) Sea State 4

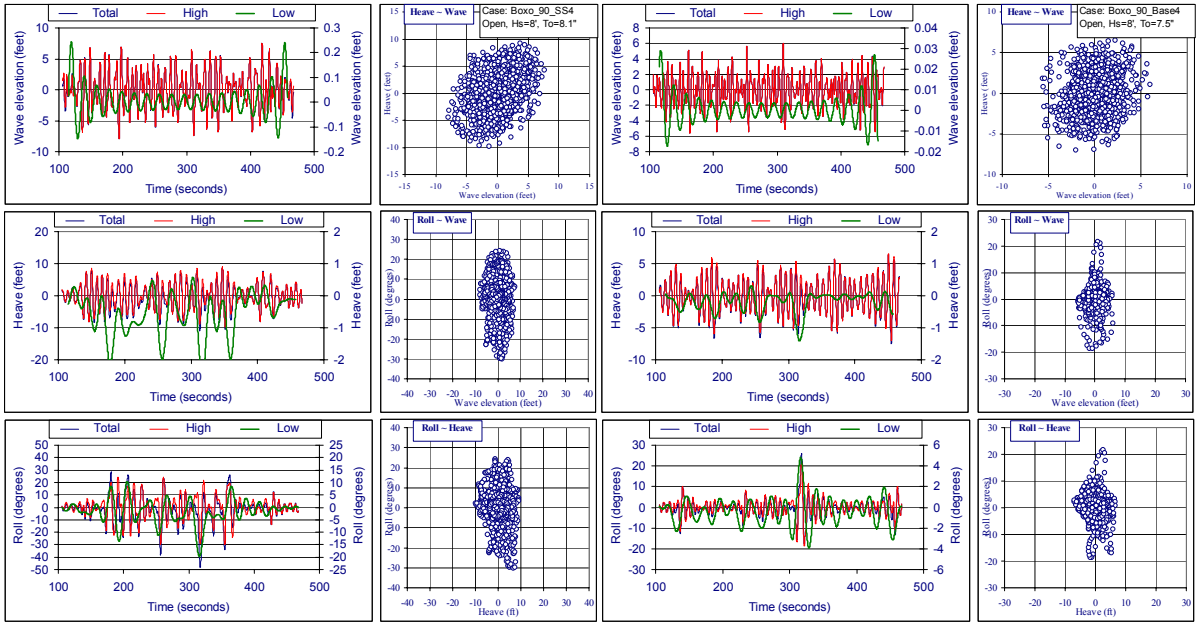


(c) Sea State 5 (d) Baseline (Hs=8', To=7.5")

Figure 43. Open box responses to: (a) Sea State 3, (b) Sea State 4, (c) Sea State 5, and (d) Baseline.

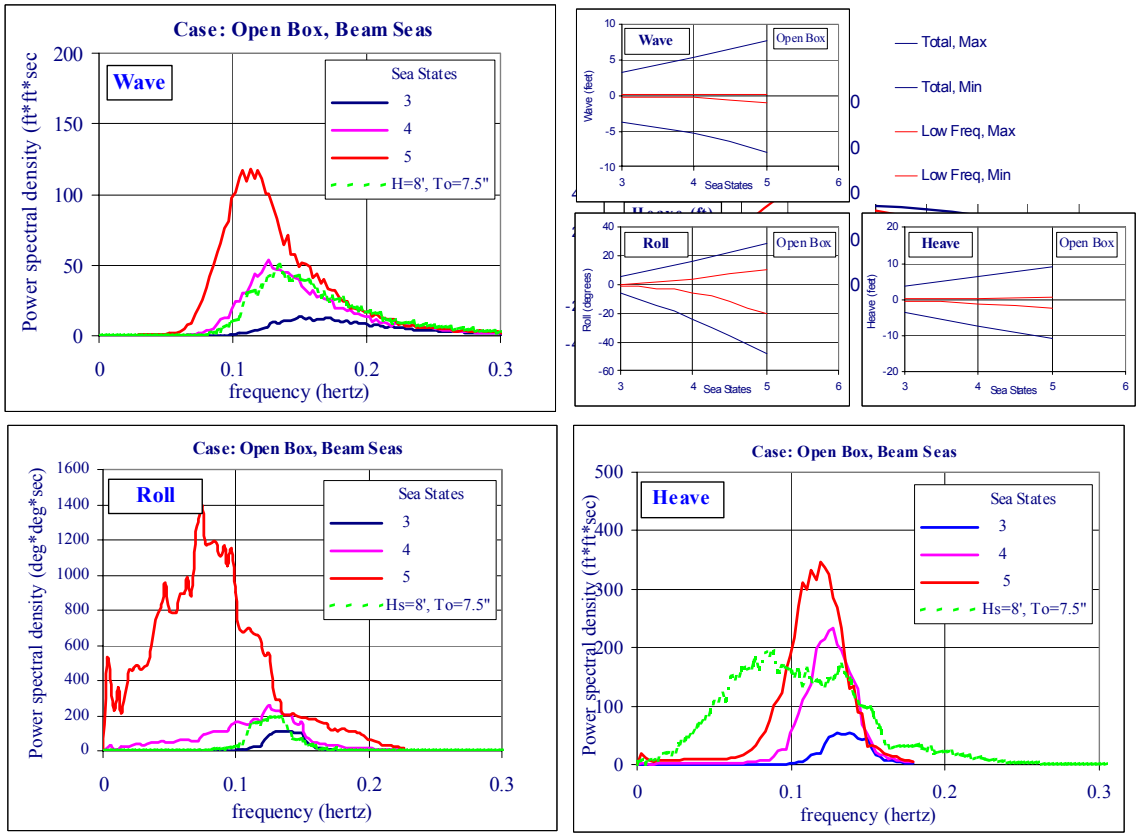


Figure 44. Threshold Sea States for open Test Bed.

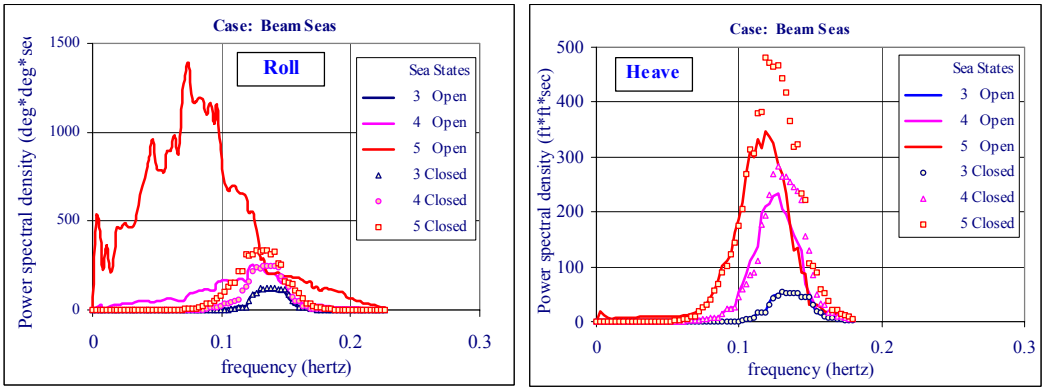


Figure 45. Comparison of seaway performance of the Open and Closed Boxes.

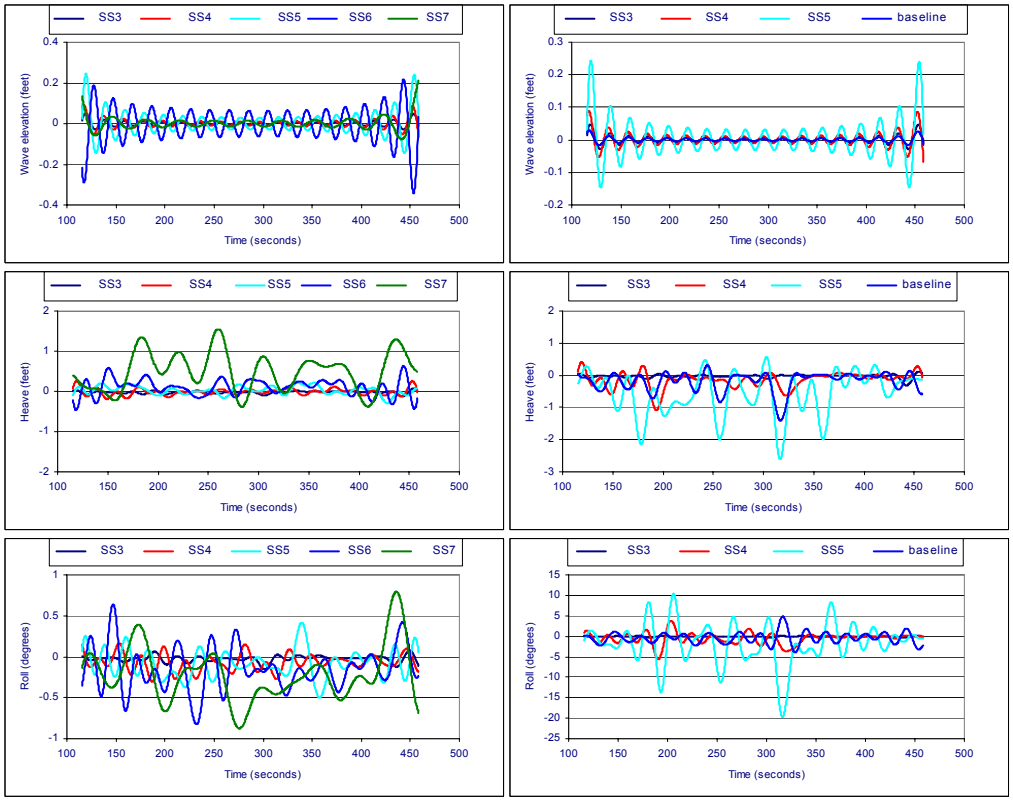


(a) Closed Box (b) Open Box

Figure 46. Low frequency drifts.

**SUMMARY**

Stability of the Test Bed has been reviewed for ocean tow along the west coast of the United States. Pertinent records of towing safety for this unique hull are scarce and the existing safety criteria do not demonstrate sufficient credibility for a full protection of this platform at all times. In fact, capsizing is a rare incident of opportunity that is heavily dependent on the time factors relevant to the random nature of seaways and vessel responses. Rational analysis is the only means to address the time factors.

Two candidate configurations of the Test Bed are considered for the ocean tow. One retains the original hull configuration as designed and the other has the space between the service and operation decks blocked and sealed watertight. Each is modeled by a rectangular box of the same envelop as its respective buoyancy hull. For this reason, they are also referred in this report as the open box and the closed box, respectively. Both boxes adopt the dimensions and mass properties deduced from the design drawings and an estimated viscous damping based on prior experience. Their dynamic performance in various seaways is fully explored with a time domain simulation model to establish a database for stability assessment. Seaways considered include theoretical seaways that are likely to excite this platform to the extreme and the realistic seaways that are expected during this ocean tow. The simulation model features the crucial capability of tracking the sensitive time factors for a fair dynamic stability assessment, including the instant wave profile, wetted hull geometry and fluid forces. This study proves that the present code is effective to distinguish concepts for critical engineering decisions.

This Test Bed is only conditionally stable because of its high center of gravity. Its wide, flat hull warrants a high initial stability, however, it also renders the platform highly sensitive to waves of 5 to 9 seconds. Heavy seas heave the platform extensively and often engulf the entire buoyancy hull. Its watertight pontoons allow the weather deck to dive deeply under water. However, severe deck immersion substantially erodes the transverse stability. Persistent deck immersion further induces extensive roll drifts. Simulation results indicate that capsizing of the open box is largely attributed to a major stability reduction due to severe deck immersion. Slow roll drifts in fact signify a probable capsizing. This slow drift stages the platform in a large list angle extensively, which subsequently couples with large down heaves to create crucial moments of very low transverse stability and renders the platform highly susceptible to the succeeding high wave groups.

Freeboard dictates the ultimate stability of this flat platform. The open box barely survives high Sea State 5. However, a theoretical seaway equivalent to low Sea State 5 is also capable of capsizing this configuration, if its peak period is in tune with the natural period of the Test Bed. The closed box significantly extends the ultimate stability above Sea State 6. This improvement is largely attributed to the additional freeboard above the service deck. In Sea State 6, this configuration rolls within 10 degrees to each side and the operation deck remains above water at all times. Therefore, capsizing is a remote concern.

Based on the simulation results, the open box configuration may be considered only if the chance of encountering seaways above 10 feet on the journey is practically zero. Otherwise, the cost to convert the Test Bed into the closed box configuration is a worthwhile insurance to this valuable asset. The open box configuration presents sufficient stability to withstand the most probable extreme seaway in the summer season along the west coast of the United States.

## REFERENCES


1. BERGER/ABAM Engineers, Inc. " Modular Hybrid Pier (MHP), Phase 2 Design Report," Volume. 1, Submitted to NFESC, Port Hueneme, CA. December 2001.

2. Huang, T., "A generalized Intact Stability Analysis Procedure for Modular Construction Platforms," NCEL Technical Note, N-1832, June 1991, Naval Civil Engineering Laboratory, Port Hueneme, CA 93043

3. Paulling, J. R., "The Transverse Stability of a Ship in a Longitudinal Seaway," Journal of Ship Research, vol. 4, No. March 1961. pp 37 – 49

4. Miller, E. R., G. C. Nickum, J. Rudnicki, and B. J. Young, "Evaluation of Current Towing Vessel Stability Criterion and Proposed Fishing Vessel Stabiity Criteria," Report prepared for U. S. Coast Guard Under Contract DOT-CG-25, 656-A, Vol. 1, Hydronautics, Incorporated. February, 1975.

5. Sarchin, T. H. and L. L. Goldberg, "Stability and Buoyancy Criteria for U. S. Naval Surface Ships," Transactions SNAME, Vol. 70, 1962

6. Goldberg, L. L., "Principle of Naval Architecture, Chapter II: Intact Stability," The Society of Naval Architects and Marine Engineers, Edited by E. V. Lewis, 1988

7. Paulling, J. R. "MULTISIM, Time Domain Platform Motion Simulation for Floating Platform Consisting of Multiple Interconnected Modules," Theoretical Manual, 3rd Edition, November 2, 1995.

8. User's Manual for the Standard Ship motion Program, SMP DTNSRDC/SPD-0936-01, David W. Taylor Naval Ship Research and Development Center, Bethesda, MD, 1981.

9. Huang, T., "Causeway Ferry Motion In Irregular Seaways", Technical Note, N-1715, November 1984, Naval Civil Engineering Laboratory, Port Hueneme, CA 93043

10. Hong, Y. S. and J. R. Paulling (1997), "A Procedure For the Com-putation of Wave- and Motion- Induced Forces on Three-dimensional Bodies at Zero Forward Speed," Prepared for ABS, 3rd Ed., October

11. Tony Cupersimith, "Preliminary Draft Report of MHP Test Bed Towing Analysis," GPC – A Joint Venture ESSM Operations, P. O. box JK, Williamsburg, VA 23187 May 25, 2004.

12. Huang, E. T., and H. C. Chen (2001), "Stability Investigation of a Pontoon Barge in Wave Basin," Proceedings, 11th ISOPE Conference, Vol. III, pp. 334-338, Stavanger, Norway, June 17-22.

## Appendix A
## Verification of Inertia and Damping Properties

Exact mass properties of a vessel are essential to any quality dynamic analysis. The elevation of the center of gravity of a ship plays a detrimental role to its ultimate stability against capsizing. For vessels of new construction or under major overhaul, mass properties are carefully calculated and documented. However, due to the extensive complexity of a ship system, even the best estimate can be significantly different from the true as-built condition. Standard inclining and free decay tests are required to confirm the necessary mass properties. From the light ship characteristics, one is able to calculate the stability characteristics of the vessel for all conditions of loading and thereby determine whether the vessel satisfies the required stability criteria. Accurate results from a stability test may, in some cases, determine the future survival of the vessel and its crew, so the accuracy with which the test is conducted cannot be overemphasized.

The free decay test further provides critical fluid-induced damping effect of a ship hull. This damping effect, if not properly included, can mislead the motion estimates of a vessel by one order of magnitude. Contractors responsible for the Test Bed construction are tasked with inclining and free decay tests upon completion to quantify the necessary mass and damping characteristics of the Test Bed as-built. The fundamentals and procedures of these two tests are summarized herein to illustrate their significance to stability analysis. The present stability analysis contains the best information available to date, but this analysis should be carefully reviewed and augmented when exact information becomes available.

### Inclining Test

A complete inclining test procedure may be found in reference A1. The determination of a vessel's light ship characteristics includes a lightweight survey and an inclining experiment. The lightweight survey involves taking an audit of all items, which must be added, deducted, or relocated on the vessel at the time of the stability test so that the observed condition of the vessel can be adjusted to the light ship condition. The weight, along with the longitudinal, transverse and vertical location of each item must be accurately determined and recorded. Using this information as well as the static waterline of the ship at the time of the stability test as determined from the freeboard at the selected locations of the vessel, the vessel's hydrostatic data, and the seawater density, the light ship displacement and longitudinal center of gravity can be obtained. The transverse center of gravity may also be calculated, if necessary.

Incline test involves moving a series of known weights, normally in the transverse direction as illustrated in Figure A1(a), and then measuring the resulting change in the equilibrium heel angle of the vessel (Figure A1(b)). By using this information and applying basic naval architecture principles, the vessel's vertical center of gravity (KG) is determined. The stability test is required for at least the first in class of most vessels upon their completion. It is normally conducted inshore in calm weather conditions. The three light ship characteristics determined from the stability test for conventional ships are displacement (disp), longitudinal center of gravity (LCG), and the vertical center of gravity (KG). Transverse center of gravity may also be determined for platforms, which are asymmetrical about the centerline or internal

arrangement, or outfitting may develop an off-center weight. The basis of determining the location of CG is briefly described in the following.

The metacenter (M) is the point around which the vessel's center of buoyancy (B) swings for small angles of inclination ($\sim 4^\circ$) as illustrated in Figure 3a. The location of B shifts to the side as the ship inclines through a small angle (θ), while its height respect to keel (K) is essentially the same. Moving a weight (W) across the deck a distance (x) will cause a shift in the overall center of gravity (GG') of the vessel equal to W(x)/Δ and parallel to the movement of W. The symbol Δ indicates ship displacement. The vessel will heel over to a new equilibrium heel angle where the center of buoyancy (B') will once again be directly under the center of gravity (G'). Because the angle of inclination during the inclining experiment is small, the shift in G can be approximated by the metacentric height, GM, and the inclination angle, θ; such that

$$\overline{GG'} = \overline{GM} \bullet \tan\theta = \frac{W(x)}{\Delta}, \quad \text{or} \qquad \overline{GM} = \frac{W(x)}{\Delta(\tan\theta)}$$

Since $\overline{GM}$ and Δ remain unchanged throughout the inclining experiment, the ratio of W(x) to tanθ will be a constant. W and x are known parameters of the test and the associated angle of inclination may be accurately measured by pendulum as shown in Figure 3b, a regression line may be established by iterating the process with various combination of upsetting moments Wx to determine GM (see Figure A1(c)). Since the location of metacenter from ship keel ($\overline{KM}$) is a simple function of hull geometry alone, it can be precisely calculated from ship lines and the draft information measured during inclining experiment. The vertical location of the center of gravity above keel $\overline{KG}$ is related to $\overline{KM}$ by the following equation as illustrated in Figure 3d. This is essentially a reverse process of calculating $\overline{GM}$ for a given ship of known $\overline{KG}$ to be described in more details in the next section.

$$\overline{KG} = \overline{KM} - \overline{GM}$$

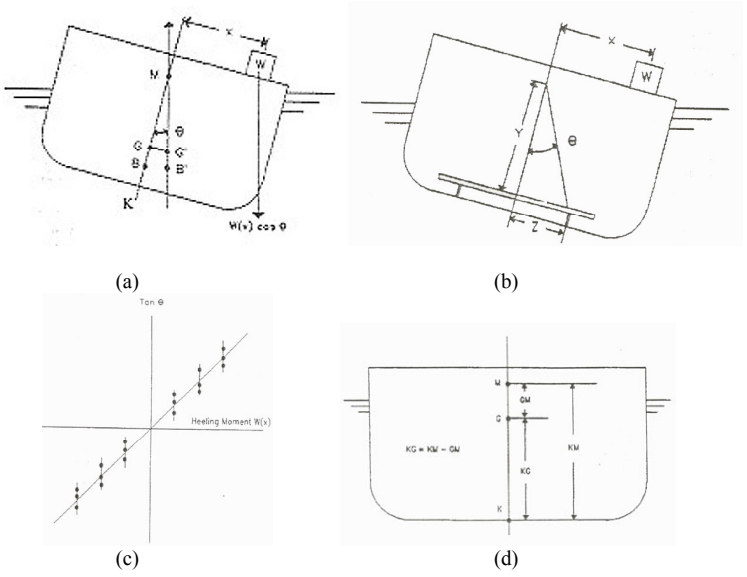


Figure A1. Inclining test.

Free Decay Test

A free-floating platform is a typical spring-mass-damper oscillator. In the absence of sustaining excitations, the platform, once disturbed, tends to oscillate about the neutral position it holds in calm water at a hull specific frequency, $\omega_d$,, and gradually damps out over time, as illustrated in Figure A2, and eventually rests in the neutral position.

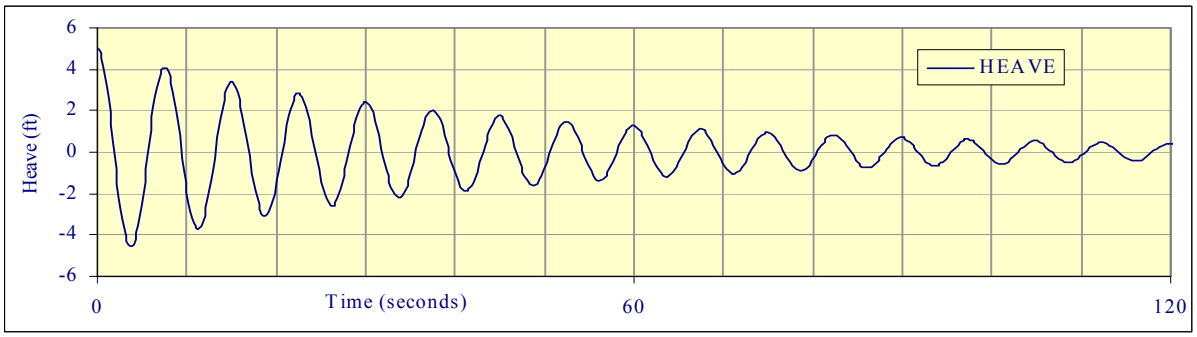


Figure A2. An example of decaying heave motion.

This motion can be described by the following equation,

$$a\ddot{x} + b\dot{x} + cx = 0$$

which we might expect the resulting oscillation be a sine wave with a continually decreasing amplitude as

$$x = X_0 \exp(-\frac{t}{\tau}) \cos(\omega_d\ t)$$

where $X_0$ is the initial deflection from the equilibrium position and the time parameter, $\tau$, is given by

$$\tau = \frac{2a}{b} = \frac{1}{\eta\omega_*}$$

and the frequency of decaying oscillation and undamped natural frequencies, $\omega_d$ and $\omega_*$ are defined as follows.

$$\omega_d = \omega_* \sqrt{(1-\eta^2)}$$

$$\omega_* = \sqrt{(\frac{c}{a})}$$

The frequency of decaying oscillation, $\omega_d$, is largely determined by the ratio of a buoyancy relevant spring constant, c, to the effective mass inertia, a, and further modified by a damping parameter, $\sqrt{(1-\eta^2)}$. This decayed frequency is slightly higher than the damped natural frequency, $\omega_0 = \omega_* \sqrt{(1-2\eta^2)}$. In the case of a small damping, this difference is negligible. The rate of motion damping, on the other hand, depends on the power consumption in wave radiation and flow separation. Unfortunately, both the effective mass and the damping of a platform are not known before hand. Although high quality viscous flow codes are now able to provide reasonable estimates, they are rarely used without further experimental confirmations. These relationships are often used in a reverse sense to validate or to determine the missing added mass and damping coefficients in the equations. This experimental process is referred to as a free decay test. In the test, a Test Bed is placed in calm water with an initial offset from its neutral position in a selected mode of motion (heave, roll, or pitch) and released without further interference. The subsequent oscillatory motion of the Test Bed similar to that of Figure 4 is then recorded for processing. When the damping is sufficiently small such that the oscillation decays very slowly; several estimates of the decay coefficient can be obtained from a single record. This method is not practical, however, when η is much greater then 0.2.

$$\eta = \frac{1}{\pi} \ln [x_{oJ} / x_{o(J+1)}]$$

where $x_{oJ}$ and $x_{o(J+1)}$ are the $J^{th}$ and $(J+1)^{th}$ extremities of the displacement histories.

The frequency of decaying oscillation $\omega_d$, may be extracted directly from the time history. The true damped natural frequency $\omega_o$ may be obtained by a multiplication factor of $\sqrt{(1-2\eta^2/(1-\eta^2)}$. Once the natural frequency and damping are determined, the added mass due to ambient water response to the platform motions at the natural frequency may also be defined.

REFERENCE

A1. ASTM, "Standard Guide for Conducting a Stability Test (Lightweight Survey and Inclining Experiment) to Determine the Light ship Displacement and Center of Gravity of a Vessel," American Society For Testing and Materials, Designation F1321 – 92 , 1992

# APPENDIX B
## Sea State Chart Compiled by Wilbur Marks of David Taylor Model Basin

### TABLE C1 GENERAL PHYSICAL DESCRIPTION OF SEA STATES

Wind and Sea Scale for Fully Arisen Sea

| Sea-General | | Wind[3] | | | | Sea[3] | | | | | | | | |
|---|---|---|---|---|---|---|---|---|---|---|---|---|---|---|
| | | | | | | Wave Height Feet | | | | | | | | |
| Sea State[1] | Description[2] | (Beaufort) Wind Force | Description | Range (knots) | Wind Velocity (knots) Average | Significant | Average 1/10 Highest | Significant Range of Periods (seconds) | $T_{max}$ (Period of Max Energy of Spectrum) | $\bar{T}$ (Average Period) | $\bar{L}$ (Average Wave Length) | Minimum Fetch (Nautical Miles) | Minimum Duration (Hours) | |
| 0 | Sea like a mirror. | 0 | Calm | Less than 1 | [a] 0 | 0 | 0 | – | – | – | – | – | – | |
| 0 | Ripples with the appearance of scales are formed, but without foam crests. | 1 | Light Airs | 1– 3 | 2 0.05 | 0.08 | 0.10 | Up to 1.2 sec | 0.7 | 0.5 | 10 in. | 5 | 18 min | |
| 1 | Small wavelets, still short but more pronounced; crests have a glassy appearance, but do not break. | 2 | Light Breeze | 4– 6 | 5 0.18 | 0.29 | 0.37 | 0.4– 2.8 | 2.0 | 1.4 | 6.7 ft | 8 | 39 min | |
| 1 | Large wavelets, crests begin to break. Foam of glassy appearance. Perhaps scattered white horses. | 3 | Gentle Breeze | 7–10 | 8.5 0.6 | 1.0 | 1.2 | 0.8– 5.0 | 3.4 | 2.4 | 20 | 9.8 | 1.7 hrs | |
| 2 | | | | | 10 0.88 | 1.4 | 1.8 | 1.0– 6.0 | 4 | 2.9 | 27 | 10 | 2.4 | |
| 2 | | | | | 12 1.4 | 2.2 | 2.8 | 1.0– 7.0 | 4.8 | 3.4 | 40 | 18 | 3.8 | |
| 2 | Small waves, becoming larger; fairly frequent white horses. | 4 | Moderate Breeze | 11–16 | 13.5 1.8 | 2.9 | 3.7 | 1.4– 7.8 | 5.4 | 3.9 | 52 | 24 | 4.8 | |
| 3 | | | | | 14 2.0 | 3.3 | 4.2 | 1.5– 7.8 | 5.6 | 4.0 | 59 | 28 | 5.2 | |
| 3 | | | | | 16 2.9 | 4.6 | 5.8 | 2.0– 8.8 | 6.5 | 4.6 | 71 | 40 | 6.6 | |
| 4 | | | | | 18 3.8 | 6.1 | 7.8 | 2.5–10.0 | 7.2 | 5.1 | 90 | 55 | 8.8 | |
| 4 | Moderate waves, taking a more pronounced long form; many white horses are formed. (Chance of some spray). | 5 | Fresh Breeze | 17–21 | 19 4.3 | 6.9 | 8.7 | 2.8–10.6 | 7.7 | 5.4 | 99 | 65 | 9.2 | |
| 5 | | | | | 20 5.0 | 8.0 | 10 | 3.0–11.1 | 8.1 | 5.7 | 111 | 75 | 10 | |
| 5 | | | | | 22 6.4 | 10 | 13 | 3.4–12.2 | 8.9 | 6.3 | 134 | 100 | 12 | |
| 5 | Large waves begin to form; the white foam crests are more extensive everywhere. (Probably some spray). | 6 | Strong Breeze | 22–27 | 24 7.9 | 12 | 16 | 3.7–13.5 | 9.7 | 6.8 | 160 | 130 | 14 | |
| 6 | | | | | 24.5 8.2 | 13 | 17 | 3.8–13.6 | 9.9 | 7.0 | 164 | 140 | 15 | |
| 6 | | | | | 26 9.6 | 15 | 20 | 4.0–14.5 | 10.5 | 7.4 | 188 | 180 | 17 | |
| 6 | | | | | 28 11 | 18 | 23 | 4.5–15.5 | 11.3 | 7.9 | 212 | 230 | 20 | |
| 6 | Sea heaps up and white foam from breaking waves begins to be blown in streaks along the direction of the wind. (Spindrift begins to be seen). | 7 | Moderate Gale | 28–33 | 30 14 | 22 | 28 | 4.7–16.7 | 12.1 | 8.6 | 250 | 280 | 23 | |
| 7 | | | | | 30.5 14 | 23 | 29 | 4.8–17.0 | 12.4 | 8.7 | 258 | 290 | 24 | |
| 7 | | | | | 32 16 | 26 | 33 | 5.0–17.5 | 12.9 | 9.1 | 285 | 340 | 27 | |
| 7 | | | | | 34 19 | 30 | 38 | 5.5–18.5 | 13.6 | 9.7 | 322 | 420 | 30 | |
| 7 | | | | | 36 21 | 35 | 44 | 5.8–19.7 | 14.5 | 10.3 | 363 | 500 | 34 | |
| 7 | Moderately high waves of greater length; edges of crests break into spindrift. The foam is blown in well marked streaks along the direction of the wind. Spray affects visibility. | 8 | Fresh Gale | 34–40 | 37 23 | 37 | 46.7 | 6–20.5 | 14.9 | 10.5 | 376 | 530 | 37 | |
| 8 | | | | | 38 25 | 40 | 50 | 6.2–20.8 | 15.4 | 10.7 | 392 | 600 | 38 | |
| 8 | | | | | 40 28 | 45 | 58 | 6.5–21.7 | 16.1 | 11.4 | 444 | 710 | 42 | |
| 8 | | | | | 42 31 | 50 | 64 | 7–23 | 17.0 | 12.0 | 492 | 830 | 47 | |
| 8 | High waves. Dense streaks of foam along the direction of the wind. Sea begins to roll. Visibility affected. | 9 | Strong Gale | 41–47 | 44 36 | 58 | 73 | 7–24.2 | 17.7 | 12.5 | 534 | 960 | 52 | |
| 8 | | | | | 46 40 | 64 | 81 | 7–25 | 18.6 | 13.1 | 590 | 1110 | 57 | |
| 9 | | | | | 48 44 | 71 | 90 | 7.5–26 | 19.4 | 13.8 | 650 | 1250 | 63 | |
| 9 | | | | | 50 49 | 78 | 99 | 7.5–27 | 20.2 | 14.3 | 700 | 1420 | 69 | |
| 9 | Very high waves with long overhanging crests. The resulting foam is in great patches and is blown in dense white streaks along the direction of the wind. On the whole the surface of the sea takes a white appearance. The rolling of the sea becomes heavy and shocklike. Visibility is affected. | 10 | Whole Gale* | 48–55 | 51.5 52 | 83 | 106 | 8–28.2 | 20.8 | 14.7 | 736 | 1560 | 73 | |
| 9 | | | | | 52 54 | 87 | 110 | 8–28.5 | 21.0 | 14.8 | 750 | 1610 | 75 | |
| 9 | | | | | 54 59 | 95 | 121 | 8–29.5 | 21.8 | 15.4 | 810 | 1800 | 81 | |
| 9 | | | | | 56 64 | 103 | 130 | 8.5–31 | 22.6 | 16.3 | 910 | 2100 | 88 | |
| 9 | Exceptionally high waves (small and medium-sized ships might for a long time be lost to view behind the waves.) The sea is completely covered with long white patches of foam lying along the direction of the wind. Everywhere the edges of the wave crests are blown into froth. Visibility affected. | 11 | Storm* | 56–63 | 59.5 73 | 116 | 148 | 10–32 | 24 | 17.0 | 985 | 2500 | 101 | |
| 9 | Air filled with foam and spray. Sea completely white with driving spray; visibility very seriously affected. | 12 | Hurricane* | 64–71 | >64 | >80[b] | >128[b] | >164[b] | 10–(35) | (26) | (18) | ~ | ~ | ~ |

This table compiled by Wilbur Marks, David Taylor Model Basin.

* For hurricane winds (and often whole gale and storm winds) required durations and fetches are rarely attained. Seas are therefore not fully arisen.

a] A heavy box around this value means that the values tabulated are at the center of the Beaufort range.

b] For such high winds, the seas are confused. The wave crests blow off, and the water and the air mix.


1) Encyclopedia of Nautical Knowledge, W.A. McEvan and A.H. Lewis, Cornell Maritime Press, Cambridge, Maryland, 1953, p. 488.

2) Manual of Seamanship, Volume II, Admiralty, London, H.M. Stationary Office, 1952, pp. 717–718.

3) Practical Methods for Observing and Forecasting Ocean Waves, Pierson, Neuman, James, N.Y. Univ. College of Engin, 1953.